JCI The Journal of Clinical Investigation

Serum- and glucocorticoid-induced kinase 3 orchestrates glucocorticoid signaling to facilitate chromatin remodeling during murine adipogenesis

Qilong Chen, … , Alexander A. Soukas, Ben Zhou

J Clin Invest. 2025. https://doi.org/10.1172/JCI186534.

Research In-Press Preview **Cell biology** **Metabolism**

Elevated glucocorticoid (GC) levels are common in conditions such as aging, chronic stress, Cushing syndrome, and GC therapy. While GCs suppress inflammation through the glucocorticoid receptor (GR), they also cause metabolic side effects. Investigating alternative pathways beyond GR activation is crucial for reducing these side effects. Our phosphoproteomics analysis revealed that glucocorticoid exposure promotes phosphorylation at the RxxS motifs of multiple proteins in preadipocytes, including those mediated by Serum- and glucocorticoid-induced kinase 3 (SGK3). SGK3 is a key mediator of glucocorticoid-induced adipogenesis, as shown by impaired adipogenesis following SGK3 inhibition or genetic ablation. *Sgk3* knockout mice were resistant to glucocorticoid- or high-fat diet-induced obesity, and PROTAC targeting SGK3 reduced adipogenesis in both obese mice and a thyroid eye disease cell line. Mechanistically, SGK3 translocated to the nucleus upon glucocorticoid stimulation, interacted with and phosphorylated the BRG1 subunit of the BAF complex, and prevented BRG1 degradation, promoting chromatin remodeling necessary for adipogenesis. These findings highlight SGK3 as a potential therapeutic target to mitigate metabolic side effects of elevated glucocorticoid levels.

Serum- and glucocorticoid-induced kinase 3 orchestrates glucocorticoid signaling to facilitate chromatin remodeling during murine adipogenesis

Qilong Chen[1#], Jialu Guo[1#], Yuyi Liu[1], Tai Du[1], Jiapei Liu[2], Yuyao Zhang[3], Yuming Dai[1], Mengdi Zhang[1], Ziqian Zhou[1], Qiyang Zhang[1], Caixia Wei[1], Qiurong Ding[1], Jun Qin[1], Qiwei Zhai[1], Ju Qiu[1], Mengle Shao[4], Fang Zhang[2*], Alexander A. Soukas[3*], Ben Zhou[1*]

[1]Shanghai Institute of Nutrition and Health, University of Chinese Academy of Sciences, Chinese Academy of Sciences, Shanghai 200031, China.

[2]National Clinical Research Center for Eye Diseases, Department of Ophthalmology, Shanghai General Hospital, Shanghai Jiao Tong University School of Medicine, Shanghai 200080, China.

[3]Department of Medicine, Diabetes Unit and Center for Genomic Medicine, Massachusetts General Hospital and Harvard Medical School, Boston, MA 02114, USA.

[4]State Key Laboratory of Immune Response and Immunotherapy, Shanghai Institute of Materia Medica, Chinese Academy of Sciences, Shanghai 200031, China.

[#]These Authors contributed equally

*Corresponding author

Address correspondence to:

Ben Zhou, Shanghai Institute of Nutrition and Health, University of Chinese Academy of Sciences, Chinese Academy of Sciences, Shanghai 200031, China. Phone: +86 021 54920762. Email: benzhou@sibs.ac.cn. Or to: Alexander A. Soukas, Department of Medicine, Diabetes Unit, Massachusetts General Hospital, Boston, MA 02114, USA. Phone: +1 6177245897. Email: asoukas@mgh.harvard.edu. Or to: Fang Zhang, National Clinical Research Center for Eye Diseases, Department of Ophthalmology, Shanghai General Hospital, Shanghai Jiao Tong University School of Medicine, Shanghai 200080, China. Phone: +86 021 63240090. Email: zhangfang2018@sjtu.edu.cn

Conflict of interest: The authors have declared that no conflict of interest exists.

Abstract

Elevated glucocorticoid (GC) levels are common in conditions such as aging, chronic stress, Cushing syndrome, and GC therapy. While GCs suppress inflammation through the glucocorticoid receptor (GR), they also cause metabolic side effects. Investigating alternative pathways beyond GR activation is crucial for reducing these side effects. Our phosphoproteomics analysis revealed that glucocorticoid exposure promotes phosphorylation at the RxxS motifs of multiple proteins in preadipocytes, including those mediated by Serum- and glucocorticoid-induced kinase 3 (SGK3). SGK3 is a key mediator of glucocorticoid-induced adipogenesis, as shown by impaired adipogenesis following SGK3 inhibition or genetic ablation. *Sgk3* knockout mice were resistant to glucocorticoid- or high-fat diet-induced obesity, and PROTAC targeting SGK3 reduced adipogenesis in both obese mice and a thyroid eye disease cell line. Mechanistically, SGK3 translocated to the nucleus upon glucocorticoid stimulation, interacted with and phosphorylated the BRG1 subunit of the BAF complex, and prevented BRG1 degradation, promoting chromatin remodeling necessary for adipogenesis. These findings highlight SGK3 as a potential therapeutic target to mitigate metabolic side effects of elevated glucocorticoid levels.

Introduction

Elevated Glucocorticoids (GC) level is a common feature in pathophysiological states, including aging, chronic stress, Cushing syndrome and GC therapy. GCs are commonly prescribed for managing inflammation in a spectrum of autoimmune, inflammatory, and allergic conditions such as thyroid eye disease, rheumatoid arthritis, lupus erythematosus, inflammatory bowel disease, transplant rejection, and asthma (1, 2). However, prolonged exposure to glucocorticoids leads to notable metabolic side effects, including central obesity, glucose intolerance, insulin resistance, and muscle mass loss (3), resembling conditions observed in individuals with excessive endogenous glucocorticoids, such as those with Cushing's syndrome. The multifaceted role of glucocorticoids in human central obesity involves promoting adipogenesis and lipid accumulation in the visceral depot of white adipose tissue (WAT) while stimulating lipolysis in subcutaneous depots (4). Moreover, chronic glucocorticoid treatment contributes to increased lipid accumulation and suppressed thermogenesis in brown adipose tissue (BAT) (5).

The effects of glucocorticoids are predominantly mediated through the glucocorticoid receptor (GR), a member of the nuclear hormone receptor family of transcription factors. Synthetic glucocorticoids like dexamethasone (DEX) are extensively used to induce adipogenesis. *In vitro* adipogenesis is usually initiated by treating post-confluent preadipocytes with the adipogenic cocktail consisting of rosiglitazone, isobutyl methylxanthine (IBMX), DEX and insulin,

collectively known as MDI. DEX rapidly binds and activates GR, leading to the expression of early adipogenic transcription factor (6). Activated GR also interacts with the histone acetyltransferase p300, promoting histone H3 acetylation and activation of enhancers for numerous adipogenic genes (7). However, recent studies have demonstrated that adipocyte GR is not required for the development of adipose tissue in mouse models (8-10). Moreover, glucocorticoids are reported to directly bind and activate certain G-protein-coupled receptors such as GPR97 (11). Hence, other glucocorticoid-activated pathways independent of GR's transcriptional activity might contribute to adipogenesis and warrant further exploration.

Adipogenesis involves orchestrated actions of transcription factors and epigenomic regulators at various differentiation stages (12, 13). Transcription factor binding to DNA often involves chromatin remodeling to enhance DNA accessibility. Mammalian SWI/SNF ATP-dependent chromatin remodeling complexes reorganize local nucleosome structures and modulate transcription factor access to their binding sites (14). SWI/SNF complexes are pivotal regulators of chromatin remodeling during adipogenesis (15-18), yet factors governing their activity remain elusive.

Mammalian Serum- and glucocorticoid-inducible kinases (SGKs) comprise three isoforms: SGK1, SGK2, and SGK3. These AGC protein kinases, functioning parallel to AKT downstream of phosphatidylinositol 3-kinase (PI3K), possess conserved catalytic activation loop and C-terminal hydrophobic motif

sites phosphorylated by PDK1 and mTORC2, respectively (19-21). SGK3, distinct from the other isoforms, is activated by both Class 1 and Class 3 PI3Ks (22). Its Phox (PX) domain facilitates SGK3 targeting to endosomal compartments and vesicle-like structures, regulating endosome function (23, 24). While SGK3 is known to regulate cell proliferation and survival (25, 26), its role in energy metabolism remains unclear. SGK3 is rapidly activated by glucocorticoid within minutes after treatment (27), suggesting its involvement in regulating pathways downstream of GC independent of GR's transcriptional activity.

Here we found that GC promptly induced phosphorylation of motifs featuring the RxxS pattern, partially mediated by SGK3. Using *Sgk3* knockout stromal vascular fraction (SVF) cells and a PROTAC targeting SGK3 degradation, we demonstrated that SGK3 promoted adipocytes differentiation. GC treatment elevated SGK3 protein levels in SVF cells, prompting SGK3 translocation to the nucleus. Nuclear SGK3 interacted with and stabilized the core SWI/SNF complex member SMARCA4 (BRG1), thereby facilitating adipogenesis via chromatin remodeling mediated by BRG1. *Sgk3* knockout mice exhibited protection from GC or high-fat diet (HFD) induced obesity, and SGK3 PROTAC also showed anti-adipogenesis effects on HFD-induced obesity, suggesting inhibiting SGK3 could potentially ameliorate GC-induced metabolic defects. Our study unveils that GC induce adipogenesis via a pathway parallel to the GR pathway, offering a promising therapeutic target for alleviating GC's side

effects.

Results

Glucocorticoids Directly Induce Phosphoproteomic Changes by Activating SGK3.

Numerous studies investigate the mechanisms of glucocorticoids' effects through GR, while recent research suggested GR-independent roles of glucocorticoids in regulating biological processes including adipogenesis. GR loss delays rather than prevents the pre-adipocyte differentiation *in vitro* (8), and does not impair the development of adipose tissue in E18 mice embryo (9). Similar to GR loss, when we induced differentiation of GR antagonist RU486 treated cells with the differentiation induction cocktail MDI, Oil Red O staining showed inhibition of GR's activity did not completely prevent pre-adipocyte differentiation (Figure 1A). The inhibitory effect by RU486 treatment was demonstrated by the totally inhibition of the upregulation of GR's downstream genes *Sgk1* and *Rasd1* by GC under both normal culture medium and steroids-free charcoal-stripped medium (Figure 1A and S1A). These results suggest other mechanisms beyond GR's function that promote adipogenesis by GCs.

To further investigate the mechanisms of GC's function beyond GR's activity, we treated primary Stromal Vascular Fraction (SVF) cells isolated from murine inguinal white adipose tissue (iWAT) with DEX shortly and found a set of proteins were phosphorylated on their serine and threonine sites after DEX

treatment in an hour (Figure 1B). Knockout of GR (*Nr3c1*) reduced but did not eliminate DEX-induced phosphorylation at serine and threonine sites, suggesting that certain protein kinases are responsive to DEX-induced protein phosphorylation independent of GR (Figure 1C). To uncover the fast responses from cells when exposed to glucocorticoid, we employed 4D-DIA proteomics and phosphoproteomics to measure total protein and phosphorylated peptides in primary SVF cells with or without DEX treatment (Figure 1D). A total of 5,747 proteins were identified, with only 92 proteins showing changes in abundance (Figure S1B), suggesting that short-term treatment with GC does not alter global protein levels. However, among approximately 15,000 quantified phospho-sites, we observed 652 upregulated phospho-sites and 649 downregulated phospho-sites (Figure 1E), indicating that GC induces rapid and widespread changes in protein phosphorylation status. Gene Ontology (GO) analysis revealed a strong correlation with protein phosphorylation-associated terms and translation-associated terms, such as chromatin organization, regulation of RNA pol II, and mRNA transport (Figure S1C). Furthermore, KEGG pathway analysis indicated enrichment of glucocorticoid-induced phospho-proteins in autophagy, cell junctions, AMPK, and insulin signaling pathways, suggesting an interaction with energy metabolism in pre-adipocytes (Figure S1D). Motif analysis of enhanced phospho-sites revealed enrichment in RxxS/T, S/TP and SDxE classes (Figure 1F), implicating activation of various protein kinase families including SGKs, AKTs, AMPK, MAPKs and CDKs. To

further validate DEX-mediated phosphorylation of RxxS/T motif-containing proteins, we conducted dose-response and time-course experiments in SVF cells. Our data revealed a clear dose- and time-dependent phosphorylation response, with RxxS/T motif phosphorylation intensity showing progressive enhancement under both elevated DEX concentrations and extended exposure durations during the first hour of treatment (Figures S2A and S2B). Moreover, other glucocorticoids including prednisolone, corticosterone and hydrocortisone similarly promote RxxS/T motif phosphorylation, mirroring the effects observed with DEX (Figure S2C). This consistent response across multiple glucocorticoids suggests a class-wide capacity to induce rapid protein phosphorylation events.

Next, to determine whether glucocorticoid-induced protein phosphorylation requires GR signaling, we examined tamoxifen-inducible GR knockout cells following DEX treatment. Strikingly, we detected sustained phosphorylation of RxxS/T motifs in specific target proteins despite complete GR ablation (Figure S2D). These findings demonstrate the existence of functional GR-independent mechanisms mediating glucocorticoid signaling. Through Gene Set Enrichment Analysis (GSEA), we identified SGK as the top-enriched kinase family (Figure 1G). Given the shared substrates among SGK family members, this finding implies the potential involvement of the three SGK family kinases in orchestrating glucocorticoid-induced phosphoproteomic alterations. Since GCs stimulate the *Sgk1* mRNA transcription through GR, and SGK3, unlike SGK1

and SGK2, has been observed to display immediate increased kinase activity upon glucocorticoid treatment (27). This prompts the hypothesis that SGK3 responses to GCs independent of GR to promote rapid phosphorylation of RxxS/T motifs. Indeed, the absence of SGK3 by treating the cells with the specific SGK3 protein degrader SGK3 PROTAC suppressed DEX-induced RxxS/T phosphorylation and the phosphorylation of NDRG1 on serine 330 (Figure 1H) without affecting GR protein level, suggesting SGK3 rapidly phosphorylates its substrates under GC treatment. Under classical conditions, SGK3 is synergistically activated by mTORC2 and the PI3K pathway in response to insulin, here our data demonstrate that DEX also activate SGK3. To determine whether distinct upstream mechanisms mediate this activation, we compared SGK3 activity in cells treated with either DEX or insulin, in the presence or absence of an SGK3 PROTAC degrader. We observed differential phosphorylation patterns of RxxS/T motif-containing proteins in response to DEX versus insulin. Notably, SGK3 PROTAC selectively abolished phosphorylation of specific bands (indicated by letter c) in DEX -treated cells but not in insulin-treated cells (Figure S2E). These findings suggest that glucocorticoids and insulin engage divergent pathways to activate SGK3. Further supporting this model, treatment with the PI3K inhibitor LY294002 only partially suppressed DEX-induced phosphorylation of RxxS/T motif-containing proteins (Figure S2F), indicating that glucocorticoids activate SGK3 through both PI3K-dependent and PI3K-independent mechanisms.

SGK3 Deficiency Protected Mice from DEX and HFD Induced Obesity.

Because one of the metabolic side effects of GC is to promote obesity, we then evaluate the function of SGK3 in regulating adipose tissue under GC treatment *in vivo.* We intraperitoneally injected 8-week-old *Sgk3*$^{-/-}$ and control *Sgk3*$^{+/+}$ male mice with DEX daily, and found *Sgk3*$^{-/-}$ mice were protected from DEX induced fat mass gain compared to control *Sgk3*$^{+/+}$ mice (Figures 2A-2C), while there was no changed splenic weight loss (Figure 2D). Similarly, female *Sgk3*$^{-/-}$ mice were also protected from DEX-induced fat mass increase (Figures 2E-2G). Thus, *Sgk3* knockout mice exhibit protection from GC-induced obesity while remaining sensitive to its immunosuppressive effects as shown by decreased spleen weight, suggesting SGK3 as a potential important target for mitigate GC induced metabolic side effects without affecting GC's immune suppression effects.

We and others found *Sgk3* knockout mice exhibit mild developmental defects, including developmental delays during infancy and adolescence (28). To mitigate the impact of developmental deficiencies observed in *Sgk3*$^{-/-}$ mice, we next employed tamoxifen-induced knock out mice by crossing *CAG*-cre^{esr1} mice with *Sgk3*$^{flox/flox}$ mice, shortly named as *Sgk3* iKO mice. In accordance with *Sgk3*$^{-/-}$ mice, we also observed lower body weight, fat mass, pgWAT weight and iWAT weight in both male and female *Sgk3* iKO mice compared with *Sgk3*$^{flox/flox}$ mice, with no significant changes in lean mass and spleen weight (Figures 2H-2O, S3A-3G). Moreover, while DEX treatment significantly induced brown fat

"whitening" and increases lipid accumulation in muscle of control animals, these adverse effects were greatly attenuated in both male and female *Sgk3* iKO mice, further indicating *Sgk3* iKO mice are protected from DEX induced metabolic side effects (Figure 2P and S3H). However, no significant differences in adipocyte size were observed in iWAT and pgWAT tissues between *Sgk3* iKO mice and *Sgk3*$^{flox/flox}$ mice (Figure 2P and S3H). These observations suggest that the distinctions in WAT tissues between *Sgk3* iKO and *Sgk3*$^{flox/flox}$ mice are not attributed to reduced adipocyte size but rather to a decreased number of adipocytes, implying that SGK3 regulates GC induced adipogenesis in preadipocyte rather than mature adipocyte *in vivo*.

A more widespread cause of obesity is over-nutrition, which induces adipogenesis in adipose tissue. A recent study also shows mice feeding with a HFD exhibit higher plasma corticosterone (29). As known the role of SGK3 in adipogenesis and DEX induced obesity, we questioned whether SGK3 deficiency can improve over-nutrition induced adipogenesis and obesity. To this aim, *Sgk3*$^{flox/flox}$ and *Sgk3* iKO mice were fed with HFD. As expected, SGK3 deficiency protected mice from HFD induced body weight gain (Figure S3I), and displayed lower fat mass, pgWAT weight and iWAT weight (Figures S3J, S3L and S3M) as well as no changed lean mass (Figure S3K). Thus, SGK3 inactivation protected mice from DEX and HFD induced obesity.

SGK3 Deficiency does not compromise normal hepatic or renal function.

Given SGK3's established roles in regulating ion channels and its critical

functions in cell survival and proliferation, we investigated whether *Sgk3* knockout affects normal hepatic and renal function, particularly during chronic DEX administration. For liver histology analysis, we measured lipid content (via Oil Red O staining), fibrosis (via α-SMA staining), and overall macroscopic changes. For kidney histopathology, we examined kidney sections for signs of fibrosis and structural abnormalities. We also measured serum liver damage markers (ALT, AST, albumin, bilirubin) and serum kidney function markers (uric acid and urea). Our results showed that DEX treatment induced hepatic lipid accumulation and a slight increase in albumin levels without altering serum markers of liver or kidney function (Figures S4A–S4F). Additionally, SGK3 deletion did not significantly affect baseline liver or kidney function, suggesting that SGK3 is dispensable for maintaining homeostasis in these organs (Figures S4G–S4L). Notably, Oil Red O staining showed DEX-induced hepatic lipid accumulation was attenuated in *Sgk3* iKO mice， with no differences in fibrosis, or serum markers of liver and kidney function between WT and *Sgk3* iKO mice (Figures S4M-S4S). These results confirmed that SGK3 deletion does not impair liver or kidney function, even after prolonged DEX treatment.

The Absence of SGK3 Prevents Preadipocyte Differentiation.

Next, we investigated whether SGK3 regulates adipogenesis *in vitro*. The upregulation of SGK3 expression during 3T3-L1 preadipocytes differentiation hints at its potential role in this process (Figures 3A and 3B). To test this hypothesis, we generated immortalized SVF cell lines with both *Sgk3* knockout

and knockdown, Oil Red O staining showed lack of SGK3 impaired adipogenesis (Figures 3C, 3D and 3F). Utilizing SGK3 protein degraders, we observed impaired adipogenesis upon SGK3 depletion in preadipocytes, corroborated by decreased lipid accumulation and reduced induction of adipogenesis markers (Figures 3E and 3F). Consistent with these findings, the SGK3 kinase inhibitor GSK650394 (5 μM) potently suppressed adipogenesis, exhibiting comparable efficacy to SGK3 PROTAC at 0.3 μM, demonstrating SGK3 kinase activity is required for its regulation on adipogenesis (Figure S5A). This effect was further validated in primary SVF cells from *Sgk3* knockout mice suggesting a cell-autonomous role for SGK3 in adipogenesis (Figure S5B). This cell autonomous effect of SGK3 on preadipocyte differentiation was further validated in FACS sorted $Lin^{-}CD29^{+}CD34^{+}Sca1^{+}CD24^{+}$ cells isolated from wildtype and $Sgk3^{-/-}$ mice, with reduced adipogenic ability observed in $Sgk3^{-/-}$ primary cells (Figure S5C). Additionally, taking advantage of SGK3 PROTAC, we treated SVF cells with PROTAC at different stages during induced adipogenesis. Early-stage SGK3 PROTAC treatment significantly impaired adipogenesis, as evidenced by Oil Red O staining and the downregulation of adipogenic marker genes including *Adipoq*, *Cebpa*, *Fabp4*, and *Pparg* (Figures 3G-3I). In contrast, late-stage treatment had only a modest effect on adipogenesis, suggesting that SGK3 regulates adipogenesis primarily during the early induction stage. Similarly, SGK3 clearance in mature adipocytes showed no differences in Oil Red O staining (Figure S5D). Together, these

results demonstrate that SGK3 is crucial for early-stage adipogenesis.

SGK3 Regulates Preadipocytes Differentiation Independent of GR.

Given GR's known involvement in adipogenesis and SGK3's rapid activation by GCs, we explored the interplay between SGK3 and the GR signaling pathway (8). To delve into the relationship between SGK3 and the GR signaling pathway, we treated control (si-Ctrl) and GR RNAi (si-*Nr3c1*) cells with or without SGK3 PROTAC. Oil Red O staining showed decreased differentiation efficiency with GR RNAi, and further reduced by SGK3 PROTAC (Figure 4A). Correspondingly, SGK3 PROTAC and RU486, a GR antagonist, had additive effect on suppressing preadipocytes differentiation evidenced by Oil Red O staining (Figure 4B). We then investigated the molecular changes in GR signaling pathway in SGK3-deficient cells. The protein level of GR remained unchanged in the absence of SGK3 (Figure 1H), as did the nuclear translocation of GR in DEX or MDI treatment (Figure 4C); *Sgk1* and *Rasd1*, known GR downstream targets, were induced to comparable levels by DEX treatment in control and SGK3 deficient cells (Figures 4D and 4E), suggesting SGK3 does not affect GR’s transcriptional regulation activity. To investigate potential additive effects of SGK3 and GR in adipogenesis regulation, we established stable cell lines constitutively expressing either empty vector or active SGK3 (S486D), combined with tamoxifen-inducible GR (*Nr3c1*) knockout. We found active SGK3 significantly enhanced adipogenesis in control cells, confirming its regulatory role in this process. While GR deficiency delayed adipogenesis in

both control and SGK3-expressing cells, the SGK3-expressing lines maintained significantly higher differentiation rates than their respective controls in both wildtype and GR deficient cells, as revealed by increased lipid droplets formation and elevated protein level of adipogenic markers Adiponectin and C/EBPα (Figures 4F and 4G). The persistence of enhanced differentiation in SGK3-expressing, GR-knockout cells demonstrated that these regulators act through distinct mechanisms, with their combined effects being additive rather than epistatic. Taken together, these findings underscore the necessity of SGK3 in adipocyte differentiation and suggest SGK3 promotes adipocyte differentiation alongside with the GR signaling pathway.

SGK3 Regulates Adipocyte Differentiation Independently of Cell Cycle-Associated Functions.

To investigate how SGK3 regulates adipogenesis, we first examined its relationship with cell cycle regulation, a critical factor in adipocyte differentiation. Proliferation of MSC or pre-adipocyte and subsequently differentiation sustains the pool of adipocyte *in vivo*. Cells undergo a specific cell cycle re-entry during adipocyte differentiation *in vivo* when fed with high fat diet, as well as induced adipocytes differentiation in cell lines *in vitro* (30). Since SGK3 regulates cell cycle in cancers (31), we questioned the impact of SGK3 absence on pre-adipocyte cell cycle-associated functions and performed EdU labeling assays *in vitro*. EdU labeling and staining revealed no changes in *Sgk3* knockout cells in proliferation (Figure S5E) or differentiation-associated cell cycle re-entry

(Figure S5F), as well as primary SVF cells isolated from wildtype and *Sgk3* iKO mice (Figures S5G and S5H). MTT assay also showed similar results in SVF cell proliferation (Figure S5I). Thus, we concluded SGK3 regulates adipocyte differentiation independently of cell cycle-associated functions. Emerging evidence highlights SGK3's crucial role in modulating arachidonic acid (AA) metabolism and catalase activity, which are key regulators of chromatin remodeling and oxidative stress that influence adipogenesis (32, 33). To investigate whether SGK3 regulates adipogenesis through these pathways, we quantified AA levels across multiple model systems. Interestingly, while we observed no significant changes in AA content in pgWAT of *Sgk3* iKO mice, we detected elevated AA levels in both iWAT of *Sgk3* iKO mice and SGK3 PROTAC-treated SVF cells (Figures S6A-S6C). This tissue-specific pattern contrasts with previous report of SGK3 promotes AA synthesis in colorectal cancer cells (32). We also measured catalase mRNA and protein levels in our model systems and found no significant differences between control and SGK3 PROTAC treated cells, or in the pgWAT tissue of WT and *Sgk3* iKO mice (Figures S6D-S6H). Together, these data suggest that the role of SGK3 does not regulate adipogenesis through regulating AA metabolism or catalase activity.

SGK3 Translocates to The Nucleus During Early Adipocyte Differentiation.

To further understand the molecular mechanism of SGK3's function in regulating adipocyte differentiation, we employed TurboID-based proximity labeling combined with MS to identify potential SGK3 interaction proteins during

adipogenesis (Figure 5A). We compared biotin labeled proteins between cells treated with MDI for 0 and 3 days. SGK3 is previously known to localize in the cytoplasm and early endosome, when activated, SGK3 is recruited to the outer membrane of early endosomes by PI(3)P via its N-terminal PX domain, phosphorylated by PDK1 and mTORC2, and fully activated(34). Consistent with its known functions, Gene Ontology (GO) cellular component analysis revealed significant enrichment of proteins localized to the cytoplasm and endosomes (Figure 5B). Unexpectedly, we also observed robust enrichment of nuclear-associated components, including the nucleus, nucleoplasm, and nuclear pore complex proteins (Figure 5B). These findings suggest potential nuclear localization of SGK3, a feature that has not been functionally characterized.

To confirm SGK3's nuclear localization, we separated nuclear and cytosolic fractions of differentiating SVF cells. The nuclear localization of SGK3 was confirmed via immunofluorescence assays on day 2 after adipocyte differentiation induction (Figures 5C) and further validated through western blotting (Figure 5D). We postulated that specific components within the MDI might trigger SGK3 translocation. Consequently, we treated SVF cells with different components of the MDI for 2 days respectively and found DEX alone sufficiently induced SGK3 nuclear translocation (Figure 5E). Although synthetic glucocorticoids like DEX primarily signal through GR (35), endogenous GCs activate both GR and MR nuclear translocation. We therefore examined whether these receptors facilitate SGK3 nuclear import. First, by using a

tamoxifen induced GR knockout cell SVF cell line (with intact MR expression), we found that MDI-induced SGK3 translocation occurred independently of GR (Fig. S7A). On the other hand, treatment with the MR inhibitor finerenone demonstrated that SGK3 nuclear translocation was also MR-independent (Fig. S7B). These results are consistent with our hypothesis that other undefined mechanisms mediate the activation of SGK3 by glucocorticoids in a receptor independent pathway.

In pursuit of understanding the mechanism driving SGK3's nuclear translocation, we examined nuclear-cytoplasmic transporter proteins among SGK3 interacting proteins (Figure S7C). Importin β1 and Exportin-1 emerged as the most enriched transporters, facilitating cargo movement from cytosol to nucleus and vice versa respectively. Thus, we speculated that SGK3 translocation might rely on the importin β complex. Co-IP assays revealed a physical interaction between SGK3 and Importin β1 (Figure 5F). Notably, MDI-induced adipogenic differentiation markedly enhanced this SGK3-Importin β1 interaction (Figure 5G). Moreover, treatment with importazole, an inhibitor of the importin β complex, effectively blocked DEX-induced SGK3 translocation (Figure 5H). Hence, glucocorticoids induce SGK3's nuclear translocation in an importin β-dependent manner.

SGK3 Is Crucial for Facilitating Chromatin Remodeling Throughout the Differentiation of Adipocytes.

Adipocyte differentiation is intricately regulated by a network of transcription factors operating within a delicately balanced chromatin landscape(13). GO biological process analysis of the SGK3 interaction proteins showed those proteins which mediate ATP-dependent chromatin remodeling were enriched among SGK3 interaction proteins (Figure 5B). And of significance, the SGK3 interaction proteins were notably enriched with components of the SWI/SNF and BAF complexes, critical for chromatin remodeling (Figure 5B). Most components of the BAF complex were identified via SGK3 TurboID proximity labeling (Figure S7D), suggesting SGK3's involvement in differentiation-associated chromatin remodeling through the BAF complex. Moreover, the protein level of the key BAF complex component SMARCA4 (BRG1) was downregulated in PROTAC-treated SVF cells. (Figure 6A). Notably, DEX-treated *Sgk3* iKO mice showed reduced expression of BAF complex components (BRG1, ACTL6A) and adipogenic markers (PPARγ, C/EBPα) in pgWAT compared to controls, without changes in GR levels (Figures S8A and S8B). While ACTL6A remained unchanged, BRG1 protein level was also decreased in pgWAT of untreated *Sgk3* iKO mice (Figure S8C). Tissue analysis revealed this BRG1 reduction was specific to pgWAT, not occurring in liver or muscle in DEX-treated *Sgk3* iKO mice (Figures S8D and S8E), demonstrating SGK3's tissue-specific control of BRG1. These results further indicate that SGK3 regulates the function of the BAF complex independently of GR protein levels.

To establish the relationship between SGK3 and the BAF complex, we used RNAi to knockdown *Brg1* in SVF cells, and treated cells with or without SGK3 PROTAC. Expectedly, BRG1-deficient cells exhibited reduced differentiation capability, which remained unaffected by SGK3 PROTAC treatment. In contrast, WT cells showed decreased differentiation capability upon SGK3 PROTAC treatment (Figure 6B). These findings suggest the reliance of SGK3 function on the BAF complex.

Next, to unravels the role of SGK3 on BRG1 chromatin occupation and subsequently chromatin remodeling landscape during early stage of preadipocyte differentiation, we conducted BRG1 CUT&TAG and ATAC-seq analyses in primary SVF cells on day 2 differentiation induction and before induction (day -3) with vehicle or SGK3 PROTAC treatment. BRG1 CUT&TAG analysis identified 4109 differential BRG1 occupied regions, of which 1158 regions were upregulated, and 2951 regions were downregulated in vehicle treated cells (Figure S8F), as well as a smaller number in SGK3 PROTAC treated cells (1550 differential occupied regions), and only 117 differential occupied regions overlapped between two conditions (Figure S8G). These results indicate that loss of SGK3 disrupts BRG1 chromatin localization during preadipocyte differentiation.

To obtain insights into the role of SGK3 on chromatin remodeling through BRG1, we further analyzed the chromatin accessibility in regions with differential BRG1 occupancy during preadipocyte differentiation. Adipogenesis is known to

involve the activation of numerous genes that facilitate preadipocyte differentiation and metabolic remodeling. The binding of the BAF complex to regulatory elements of these genes aids in their activation. Accordingly, pathway analysis of genes near regions with enhanced BRG1 occupancy revealed enrichment in terms related to white fat cell differentiation and adipogenesis (Figure 6C). We focused on these loci with enhanced BRG1 binding and observed that the loss of SGK3 diminished BRG1 occupancy at these sites, indicating that SGK3 is necessary for BRG1 chromatin localization during adipogenesis (Figures 6D and 6E). Consequently, the chromatin accessibility of these loci also reduced by loss of BRG1 binding caused by the absence of SGK3 (Figures 6D and 6E). These results suggest that the transcriptional program of preadipocyte differentiation is disrupted by the loss of SGK3 through the disruption of BRG1 chromatin localization on adipogenesis-associated genes. Consistent with these observations, similar changes in BRG1 occupation and chromatin accessibility were observed at *Cebpa* and *Pparg* gene loci, which are master transcription factors of adipogenesis (Figure 6F). Together, these results underscore the dependency of SGK3 function on chromatin remodeling during preadipocyte differentiation via BRG1.

SGK3 Interacts with BRG1 And Regulates Its Protein Level via The Ub-Proteasome System.

Our subsequent objective was to uncover SGK3's influence on chromatin

remodeling through the BAF complex. We conjectured that the regulation of the BAF complex by SGK3 might depend on particular components within the complex. Given BRG1's prominence in SGK3 interactions with the BAF complex, we speculated that SGK3 governs the BAF complex via BRG1 (Figure S7D). To verify this, we conducted co-immunoprecipitation (co-IP) and GST pull-down assays. The co-IP assay confirmed the interaction between SGK3 and BRG1 in differentiating SVF cells (Figure 7A). Additionally, the GST pull-down assay utilizing purified GST or GST-SGK3 proteins as baits, distinctly revealed the presence of the BRG1 protein band in the GST-SGK3 pull-down assay, affirming a direct interaction between SGK3 and BRG1 (Figure 7B).

We further confirmed that BRG1 protein levels were upregulated in SGK3-overexpressing cells while downregulated in SGK3-deficient cells (Figure 7C). *Brg1* mRNA levels remained unaffected in SGK3-deficient cells (Figure 7D). These results suggested that SGK3 regulates BRG1 expression in a post-transcriptional manner, thus we examined the BRG1 protein stability. Indeed, the stability of BRG1 protein was reduced in SGK3-deficient cells compared to vehicle treated cells (Figure 7E) when translation was inhibited by Cycloheximide (CHX) treatment, and this change could be restored by bortezomib treatment, an inhibitor of proteosome (Figure 7F). To investigate whether SGK3 kinase activity regulates BRG1 stability, we reconstituted *Sgk3* KO SVF cells with either constitutively active SGK3 (SGK3 S486D) or a kinase-dead mutant (SGK3 K191A) (28, 36). Under CHX treatment, we observed that

BRG1 degradation was significantly accelerated in *Sgk3* KO cells compared to controls, and overexpression of active SGK3 rescued BRG1 stability while the kinase-dead mutant failed to prevent BRG1 degradation (Figure 7G). These results demonstrate that SGK3's kinase activity is essential for maintaining BRG1 protein stability. Together with the observation of elevated poly-ubiquitination of BRG1 in SGK3-deficient cells (Figure 7H), we speculate that SGK3 modulates BRG1 stability via ubiquitination-proteosome pathway.

SGK3 Directly Phosphorylates BRG1.

Given the kinase nation of SGK3, we aimed to explore whether SGK3 regulates BRG1 stability through phosphorylation. With several RxxS/T substrate motifs present in the BRG1 protein sequence, we assessed BRG1 phosphorylation levels using an antibody against Rxx-p-S/T in an *in vitro* kinase assay. The result displayed an increased phosphorylation level of BRG1 protein upon incubation with SGK3 S486D (Figure 7I). Subsequent mass spectrometry experiments explored the 428-threonine site (accord with RxxS/T motif) and 1417-serine site (accord with KxxS/T motif, non-classic substrate motif of SGK3) of human BRG1 was phosphorylated in the *in vitro* assay (Figure 7J). These two sites are also conserved in mouse BRG1 protein as 428-threonine and 1384-serine. Next, we sought to determine whether ubiquitination and protein stability of BRG1 controlled by phosphorylation of T428/S1417. Indeed, T428A/S1417A mutant of BRG1 displayed increased ubiquitination level and instability (Figures 7K and 7L).

Collectively, these findings provide evidence of a GR-independent glucocorticoid-SGK3-BRG1 axis governing chromatin remodeling crucial for adipocyte differentiation *in vitro*.

SGK3 Deficiency in Adipocyte Progenitors Improves DEX-Induced Obesity

To investigate the potential role of SGK3 in protecting against DEX-induced obesity within mature adipocytes, we created mature adipocyte-specific *Sgk3* knock out mice by breeding *Adipoq*-Cre mice with *Sgk3*$^{flox/flox}$ mice (Figure S9A). These mice, termed *Sgk3* AKO mice, were created to explore SGK3's function beyond adipocyte differentiation. Analysis of body weight, fat mass, lean mass, iWAT weight, pgWAT weight, and liver weight revealed no differences between *Sgk3* AKO mice and *Sgk3*$^{flox/flox}$ mice under both DEX-treated and HFD conditions (Figures S9B-S9O). These findings suggested that the beneficial effect of SGK3 deficiency in mitigating glucocorticoid-induced obesity is independent of mature adipocytes.

Having demonstrated impaired adipocyte differentiation in SGK3-deficient cells *in vitro*, we further investigated SGK3's functional role *in vivo* by generating adipocyte progenitor-specific knockout (APKO) mice through the crossbreeding of *Pdgfrα*-Cre mice with *Sgk3*$^{flox/flox}$ mice, shortly named as *Sgk3* APKO mice. The knockout efficiency was demonstrated by western blotting of SGK3 in both pgWAT and iWAT (Figure S10A). 8-week-old *Sgk3* APKO mice and *Sgk3*$^{flox/flox}$ mice were intraperitoneally injected with dexamethasone. After 35 days, *Sgk3*

APKO mice also displayed lower body weight, reduced fat mass and decreased pgWAT weight compared with *Sgk3*$^{flox/flox}$ mice (Figures S10B-S10F). These observations supported the function of SGK3 in adipocyte progenitors *in vivo*. Moreover, we examined adipose tissue development in *Sgk3* APKO mice. *Sgk3* APKO neonates (postnatal day 5) exhibited reduced iWAT mass compared to controls (Figure S10G), indicating that SGK3 plays a regulatory role in early iWAT adipogenesis *in vivo*. The formation of adipose tissue, albeit at reduced efficiency, demonstrates that SGK3 is not essential for adipogenesis. Together, these findings position SGK3 as a facilitator of adipogenesis.

Given the above, our study proved the requirement of SGK3 in glucocorticoid induced obesity in mice. The protective function observed in *Sgk3* knockout mice was partially reliant on adipocyte progenitors, as previously mentioned, rather than on mature adipocytes.

SGK3 Deficiency Inhibits Adipogenesis *in Vivo*

Finally, to further substantiate SGK3's role in regulating adipogenesis *in vivo*, we employed AdipoChaser mice to investigate whether SGK3 deficiency indeed inhibit adipocyte differentiation *in vivo*. AdipoChaser mice were generated by crossing *Adipoq-rtTA*, *TRE-cre*, *Rosa26*-STOP-*lacZ*, wherein mature adipocytes express LacZ upon doxycycline administration, but the newly developed adipocytes are negative of LacZ (37). This model allowed us to label existed mature adipocyte, and to identify newly developed adipocyte after 1 month of dexamethasone administration, with or without SGK3 PROTAC

treatment. We induced Cre activity of WT AdipoChaser mice by 1 week doxycycline administration, and started DEX administration a week later. Concurrently with the DEX regimen, we injected SGK3 PROTAC into the right part of iWAT to induce SGK3 degradation every two days, using vehicle as a control in the left part (Figures S10H and S10I). After 1-month treatment, iWAT tissues were collected and stained. Sections revealed a greater number of blue-stained adipocytes in the right part compared to the left part of the iWAT tissues (Figure S10J), indicating impaired adipogenesis in SGK3 deficient iWAT tissues. To further confirm this, we similarly performed experiments using the AdipoChaser-*mT/mG* mouse model, in which doxycycline induction labels pre-existing adipocytes with GFP (green) and newly generated adipocytes with tdTomato (red), enabling clearer quantification (Figure 8A). Quantitative analysis showed comparable ratios of green (mature) to red (new) adipocytes in iWAT between control and SGK3 PROTAC treated parts under basal conditions. However, DEX treatment induced a significant increase in adipogenesis in control iWAT, while this response was substantially blunted in SGK3 PROTAC treated iWAT (Figure 8B). Furthermore, immunohistochemical analysis of cleaved caspase-3 in adipose tissue revealed no differences in apoptotic activity between DEX -treated and control groups, nor between vehicle and SGK3 PROTAC treatment (Figure S10K), suggesting the change of adipocytes is not because of cell apoptosis. Together, these findings demonstrate that SGK3 regulates white adipose tissue adipogenesis in vivo.

Pharmaceutical Targeting of SGK3 Attenuates HFD-induced Obesity in Mice

Next, we studied whether pharmaceutical inhibition of SGK3 could improve obesity. To monitor the development of obesity, we fed mice with HFD for 2 weeks, followed by vehicle or SGK3 PROTAC injections every 2 days. A control group of mice was fed a chow diet and received vehicle injections (Figure 8C). After 8 weeks of treatment, the HFD-PROTAC group showed lower body weight, fat mass, pgWAT, and iWAT mass compared to the HFD-vehicle group, with no change in lean mass (Figures 8D-8J). We also performed glucose and insulin tolerance tests in HFD-fed mice treated with SGK3 PROTAC to assess their metabolic effects. Our results demonstrate that SGK3 PROTAC markedly improved both parameters compared to untreated controls (Figures S11A and S11B). Overall, these results suggest that pharmaceutical targeting of SGK3 can attenuate HFD-induced obesity.

To test the therapeutic potential for treating already obese animals, we treated *ob/ob* mice with SGK3 PROTAC for 6 weeks and checked the phenotypes. Although SGK3 PROTAC did not reduce fat mass in *ob/ob* mice, it significantly improved glucose and insulin tolerance (Figures S11C-S11J). This suggests that targeting SGK3 degradation may have therapeutic potential for metabolic dysfunction in obesity, independent of changes in adiposity. The absence of fat mass reduction implies that the metabolic benefits of SGK3 PROTAC are mediated through SGK3's function in non-adipocyte cell types, which need

further exploration.

SGK3 Regulates Human Preadipocyte Differentiation

To further examine whether the function of SGK3 in preadipocyte differentiation is conserved between mice and human, we utilized an immortalized human fibroblast cell line derived from the orbital adipose tissue of a patient with thyroid eye disease (TED). We then induced differentiation of these cells with or without SGK3 PROTAC treatment. Consistently, SGK3 PROTAC treatment inhibited preadipocyte differentiation and lipid accumulation, as indicated by significantly reduced BODIPY intensities (Figure 8K and 8L). Additionally, western blot analysis showed that adipogenesis markers ACC1 and C/EBPα, as well as BRG1, were significantly downregulated in differentiating human preadipocytes (Figure 8M).

In summary, our study unveiled GC-induced SGK3 activation in adipocyte progenitors. SGK3 deficiency impaired adipocyte differentiation both *in vitro* and *in vivo*, and consequently ameliorated GC-induced obesity in mouse model. More importantly, pharmaceutical targeting of SGK3 attenuated HFD-induced obesity in mice, and the role of SGK3 in regulating adipogenesis is conserved between humans and mice. Mechanistically, we uncovered the translocation of SGK3 to the nucleus upon glucocorticoid exposure, a process reliant on the importin β complex. Nuclear SGK3 phosphorylated BRG1, the core subunit of the BAF complex, and maintained BRG1 protein stability. In the absence of SGK3, BRG1 expression decreased, leading to compromised chromatin

remodeling required for adipocyte differentiation (Figure S11L).

Discussion

Glucocorticoids (GCs) primarily exert their function through the glucocorticoid receptor (GR), yet other pathways beyond the GR pathway can also be activated by GCs. For instance, GCs have been shown to directly bind and activate GPR97, although its downstream signaling remains elusive (11). Several studies have demonstrated that GR accelerates but is dispensable for GC induced adipogenesis (8-10), suggesting the involvement of other pathways. In this context, we proposed a non-canonical pathway through which GCs regulate adipogenesis in parallel to GR. Our findings reveal that GCs rapidly induce global changes in protein phosphorylation, partially mediated by the nutrient- and growth factor-responsive kinase SGK3. We demonstrate a mechanism by which SGK3 contributes to GC-induced adipogenesis through the phosphorylation of the core subunit BRG1 within the chromatin remodeling SWI/SNF complex. Moreover, our results from *Sgk3* knockout mice showed protection against GC-induced obesity while retaining sensitivity to GCs' immune suppression effects, highlighting SGK3 as a potential therapeutic target for addressing the metabolic side effects of GCs.

Numerous studies have demonstrated that glucocorticoids (GCs) induce epigenetic alterations by activating their receptor, GR. For instance, GR recruits CBP and HDAC1 to target promoter sites by interacting with the RelB/p52 transcription factor, leading to dynamic acetylation and deacetylation of H3K9

(38). Additionally, GCs can promote chromatin remodeling, altering the accessibility of GR-binding sites to the transcriptional machinery (39). Our findings here reveal a novel mechanism by which GCs regulate chromatin accessibility through modulating the stability of the core SWI/SNF complex subunit, BRG1. Chronic GC treatment not only activates SGK3 but also induces its nuclear translocation, where it binds to BRG1 and directly phosphorylates it. This phosphorylation of BRG1 by SGK3 during adipocyte differentiation confers resistance to ubiquitination-mediated protein degradation, thereby promoting chromatin remodeling for the expression of key adipogenesis genes. Further investigations are necessary to explore whether these phosphorylation sites also regulate other components of the SWI/SNF complex and their interactions with chromatin.

Both Class 1 and Class 3 PI3Ks act as positive regulators of adipogenesis (40, 41). SGK3 kinase activity is activated by both Class 1 and Class 3 PI3Ks (22) and is also induced by GC treatment (27), highlighting SGK3's pivotal role in adipogenesis regulation. Indeed, our findings demonstrated that knockout of *Sgk3* or degradation of SGK3 using SGK3 PROTAC significantly impairs adipocyte differentiation. NDRG1, a substrate of SGK family kinases (including SGK1, SGK2, and SGK3), has been reported to activate adipogenesis by promoting the transcription of key adipogenic genes (42). Our results indicate that, in addition to NDRG1, SGK3 directly alters chromatin status by phosphorylating the core subunit BRG1 of the chromatin remodeling SWI/SNF

complex. Therefore, under adipogenic stimuli, SGK3 likely coordinates multiple pathways, including Class 1 and Class 3 PI3Ks, mTORC2, and glucocorticoid-activated pathways, leading to global gene expression changes necessary for adipocyte differentiation. We observed SGK3's nuclear localization after chronic GC treatment, despite its typical endosomal localization. While Importin β1 is known to mediate SGK3 translocation into the nucleus, the detailed mechanism of SGK3 shuttling between the cytoplasm and nucleus requires further exploration.

Specifically knocking out of *Sgk3* in mature adipocytes using *Adipoq*-Cre has no effect on dexamethasone induced fat accumulation. Our *in vitro* data also show downregulation of SGK3 by SGK3 PROTAC treatment does not inhibit adipogenesis post the induction stage under adipogenic MDI treatment, Together, these findings suggest that SGK3 primarily regulates the early phase of adipogenesis. However, adipocyte progenitors specific *Sgk3* knockout mice using *Pdgfrα*-Cre do not fully phenocopy the global *Sgk3* knockout mice under chronic GC treatment, implying the involvement of SGK3 in other cell types as well. Given SGK3's role in regulating insulin secretion in islet beta-cells (43), further investigation into SGK3's function in other tissues under GC treatment would be valuable.

Our data reveal that *Sgk3* knockout mice exhibit substantial protection against chronic glucocorticoid-induced obesity while remaining sensitive to GC's immunosuppressive effects. Since GCs are commonly used to treat

inflammatory diseases, addressing their metabolic side effects is critical for patient management. Our findings suggest that SGK3 could serve as a potential therapeutic target to mitigate these metabolic complications without compromising the anti-inflammatory efficacy of GCs. Additionally, SGK3 PROTAC shows promise as a tool for targeting SGK3, with our experiments demonstrating improved outcomes in HFD-fed mice, including reduced body weight, fat mass, and decreased weight of pgWAT and iWAT. These results underscore SGK3 as a viable pharmacological target for managing GC or over-nutrition-induced obesity. Further investigation is worth doing to clarify the treatment benefits in the context of chronic GC application. Notably, SGK3 PROTAC treatment in *ob/ob* mice significantly improved glucose homeostasis and insulin sensitivity (Figures S11C-S11J), despite unchanged adiposity. These findings demonstrate that SGK3 inhibition can ameliorate obesity-associated metabolic dysfunction independent of fat mass reduction.

The marked metabolic benefits conferred by SGK3 inhibition under both DEX and HFD challenge establish it as a promising therapeutic target for glucocorticoid-induced and obesity-related metabolic disorders. Due to its widespread expression and involvement in diverse physiological processes, the safety profile of SGK3 inhibition requires thorough evaluation. In metabolism, SGK3 contributes to glucose homeostasis, as *Sgk3*/*Akt2* double-null mice exhibit impaired glucose tolerance, reduced plasma insulin, and diminished β-cell proliferation, highlighting its role in pancreatic islet function (43). SGK3 also

modulates intestinal glucose absorption via the SGLT1 transporter (44). However, *Sgk3* knockout mice retain normal glucose homeostasis under baseline conditions, although these mice display wavy fur and curly vibrissae due to keratinocyte defects (28, 43), suggesting functional redundancy in metabolic regulation. Beyond metabolism, SGK3 governs ion transport systems, including calcium-phosphorus metabolism through phosphorylation of TRPV5/6 channels (45, 46). Phenotypic studies of *Sgk3* knockout mice reveal mild skeletal effects (subtly reduced bone density and phosphaturia) without major renal or calcium excretion abnormalities. The therapeutic potential of SGK3 inhibition has been particularly promising in oncology, where it overcomes drug resistance in HER2+ breast cancer and counteracts rapamycin resistance via mTORC1 reactivation (26, 47). These beneficial effects with the mild phenotypes in knockout models, suggesting that systemic SGK3 inhibition may be well-tolerated. Our finding that SGK1 protein levels are elevated in the adipose tissue of *Sgk3* iKO mice suggests functional compensation by other SGK family members, which may mitigate potential toxicity risks. Together with observations from our and other labs showing that *Sgk3* knockout mice maintain normal growth, development, and adult metabolic parameters, with only transient developmental delays (28), these findings suggest SGK3 as a promising therapeutic target with a favorable safety profile.

In summary, our results highlight the critical role of SGK3 in GC-induced chromatin remodeling and adipogenesis. SGK3 appears to function as a central

hub integrating signals from GCs and growth factors like insulin, thereby promoting adipocyte differentiation through the regulation of epigenetic alterations. The retained immune suppression function of GCs in *Sgk3* knockout mice suggests that modulating SGK3 expression could be a relevant target for mitigating the metabolic side effects of GCs.

Methods

Sex as a biological variable

Our study examined male and female animals, and similar findings are reported for both sexes.

Animals

Sgk3 global knockout mice (*Sgk3*$^{-/-}$) were obtained from C57BL/6 zygotic injection of small guide RNAs targeting *Sgk3* and S.p.Cas9 mRNA at the Genome Modification Facility, Harvard University (48). *Sgk3*$^{flox/flox}$ mice (STOCK No. S-CKO-03505**)** were obtained from Cyagen. *Nr3c1*$^{flox/flox}$ mice (STOCK No. NM-CKO-200201) were obtained from SHANGHAI MODEL ORGANISMS. The *CAG*-Cre^{esr1} (Stock No: 004682), *Pdgfrα*-Cre (Stock No: 013148) mice were obtained from the Jackson laboratory. *Adipoq*-Cre mice were kindly provided by Dr. Qiurong Ding from Shanghai Institute of Nutrition and Health, Chinese Academy of Sciences. Inducible *Sgk3* global knock out mice (*Sgk3* iKO), Adipocyte progenitor specific *Sgk3* knock out mice (*Sgk3* APKO) and mature

adipocyte specific *Sgk3* knock out mice (*Sgk3* AKO) were obtained by breeding *Sgk3*$^{flox/flox}$ mice with *CAG*-Cre^{esr1}, *Pdgfrα*-Cre and *Adipoq*-Cre mice respectively. To induce Cre activity of *Sgk3* iKO mice, tamoxifen dissolved in coin oil was intraperitoneally injected at a dose of 75 mg/kg for 5 consecutive days. The *Adipoq-rtTA*; *TRE-cre*; *Rosa26*-STOP-*lacZ* AdipoChaser mice were kindly provided by Dr. Fang Zhang from Shanghai General Hospital, Shanghai Jiao Tong University. The *Adipoq-rtTA; TRE-Cre; ROSA26-mT/mG* AdipoChaser mice were kindly provided by Dr. Mengle Shao from Shanghai Institute of Immunity and Infection, Chinese Academy of Sciences. To induce Cre activity of AdipoChaser mice, doxycycline hyclate were supplemented into drinking water at a dose of 1mg/mL for 7 days. The SGK3 PROTAC was dissolved in 3.5% DMSO/2.1% Tween 80/PBS. For injection into the iWAT, 50 μL of vehicle or SGK3 PROTAC emulsion were injected into the left or right side every 2 days, starting 1 week after Cre induction. Water soluble dexamethasone at a concentration of 1 mg/mL in PBS was intraperitoneally injected at a dosage of 5 mg/kg/day for 8-week-old mice or as otherwise specified. High-fat diet was fed to 6-week-old mice or as otherwise indicated. For SGK3 PROTAC treated HFD fed mice, 6-week-old mice were first fed HFD for 2 weeks, followed by intraperitoneal injections of SGK3 PROTAC at a dose of 15 mg/kg every two days for 8 weeks unless otherwise specified.

All mouse strains were maintained on a C57BL/6J background. Sibling or age matched mice were used for all the experiments. All mice experiments were

approved by the Institutional Animal Care and Use Committee of the Shanghai Institute for Nutrition and Health, Chinese Academy of Sciences. All mice were housed in temperature-controlled, specific pathogen-free barrier facility under a 12 hr light-dark cycle.

Cell culture and treatments

HEK293T cell line was obtained from the Cell Bank, Type Culture Collection Committee, Chinese Academy of Sciences and cultured in DMEM supplemented with 10% FBS and 1% penicillin/streptomycin in a humidified incubator with 5% CO_2 at 37 °C. Immortalized WAT SVF cells were kindly provided by Dr. Qiurong Ding from Shanghai Institute of Nutrition and Health, Chinese Academy of Sciences. and cultured in DMEM supplemented with 20% FBS and 1% penicillin/streptomycin in a humidified incubator with 5% CO_2 at 37 °C. To induce differentiation of immortalized WAT SVF cells into adipocytes, cells were cultured in DMEM supplemented with 10% FBS until they reached confluence. They were then treated with the adipogenic cocktail MDI (0.5 mM IBMX, 1 μM dexamethasone, 1 μM rosiglitazone, 5 μg/mL insulin) for 48 hours, followed by maintenance in 5 μg/mL insulin for 4-6 days. Primary SVF cells were isolated from iWAT of wild-type, *Nr3c1*$^{flox/flox}$ or *CAG*-Cre^{esr1} *Nr3c1*$^{flox/flox}$ mice. Briefly, mice were sacrificed, and iWAT tissues were collected, washed with PBS, minced into small pieces, and digested with 300 U/mL collagenase I at 37°C for 30 min. The resulting cell suspension was filtered through a 70 μm strainer, centrifuged, and the pellet was collected and seeded. The medium

was changed after 4 hours, and cells were maintained in DMEM/F12 supplemented with 10% FBS. SVF cells derived from *CAG*-Cre^{esr1} *Nr3c1*$^{flox/flox}$ mice were immortalized through lentiviral transduction of the SV40 large T antigen. To induce differentiation into adipocytes, cells were cultured in DMEM/F12 supplemented with 10% FBS until they reached confluence. They were then treated with the adipogenic cocktail MDI (0.5 mM IBMX, 1 μM dexamethasone, 5 μg/mL insulin, 2.5 μM rosiglitazone) for 72 hours, followed by maintenance in 5 μg/mL insulin for 4-6 days. The SGK3 PROTAC were dissolved in DMSO and added to the culture medium at a final concentration of 0.3 μM at the indicated time points. For glucocorticoid treatment, cells were cultured with 1% FBS overnight or cultured with 5% CS-FBS as indicated in figure legends. CS-FBS was prepared by incubating FBS with dextran coated charcoal overnight, followed by filtration through a 0.22 μm membrane. To inhibit GR activity, RU486 was added to the culture medium at a final concentration of 10 μM, either 30 minutes before DEX treatment or throughout preadipocyte differentiation. The human immortalized preadipocyte cell line was kindly provided by Dr. Fang Zhang, Shanghai General Hospital, Shanghai Jiao Tong University School of Medicine, and was cultured and induced to differentiate as previously reported (49). The cells were cultured in DMEM/F12 supplemented with 10% FBS and 1% penicillin/streptomycin. To induce differentiation into adipocytes, cells were cultured in DMEM/F12 supplemented with 10% FBS until they reached confluence. They were then treated with the

adipogenic cocktail MDI (0.5 μM IBMX, 1 μM dexamethasone, 5 μg/mL insulin, 2.5 μM rosiglitazone) for 72 hours, followed by maintenance in 5 mg/mL insulin and 2.5 mM rosiglitazone for another 10 days.

Statistics

All quantifications of adipocyte area were conducted using ImageJ. Statistical analyses were performed using GraphPad Software. The statistical differences between control and experimental groups were determined by two-tailed T-test (two groups), one-way ANOVA (for more than two groups), or two-way ANOVA (for two independent experimental variables), with corrected P values < 0.05 considered significant. Asterisks denote corresponding statistical significance (*p < 0.05; **p < 0.01; ***p < 0.001 and ****p < 0.0001). The statistical tests performed and definition of “n” numbers in this study are indicated in the figure legends. EdgeR was used for statistical differences of BRG1 occupied regions. For Figures 2A-2P, 8B-8G, S3A-S3E, S7B-S7I and S8B-S8F, “n” represents the number of mice. For Figures 1A, 3I, 4D-4E, 5G, 6A, 7D-7F, 7J, 8I-8J and S3H, “n” represents the number of cells that were analyzed. For Figures 3B-3E, 3H, 4A-4B, 5D, 6B, and S4C, “n” represents biological replicates. For Figure S4D-S4G, “n” represents analyzed microscopic fields. For Figure 6E, “n” represents number of analyzed genomic foci. For cell culture western blotting, each sample within each biological replicate corresponds to one well from a tissue culture plate. For mouse adipose tissue western blotting, each sample corresponds to protein extract from one mouse.

Study approval

All animal studies were approved by the Institutional Animal Care and Use Committee of Shanghai Institute of Nutrition and Health (SINH-2022-ZB-2).

Data Availability

Values for all data points in graphs are reported in the Supporting Data Values file. The BRG1 CUT&TAG and ATAC sequencing data generated in this study are available in GSE268382.

Author contributions

Q.C., F. Z., A.A.S. and B.Z conceived the project. Q.C. and B.Z wrote the manuscript. Q.C., J.G., Y.L., T.D., J.L., Y.Z., Y.D. Q.Z., Z.Z., M.Z., C.W. and B.Z. performed experiments and analyzed results. Q.D., Q.Z., J.Q., J.Q., M.S., F.Z. and A.A.S. contributed to the discussion and edited the manuscript.

Acknowledgements

We thank Yufeng Ding, Weijun Pan, Yu Li, Jun Qin for discussions and sharing reagents, thank Zhonghui Weng, Cheng Wang, Zhigang Li, Zi Li, Yifan Bu, Feng Zhao and Jiayu Wu from Institutional Center for Shared Technologies and Facilities of SINH, CAS for technical assistance, and the staff members of the Mass Spectrometry System at the National Facility for Protein Science in

Shanghai (NFPS), Zhangjiang Lab, China for providing technical support and assistance in data collection and analysis. This work was supported by grants from the National Key R&D Program of China (2023YFA1801100), the National Natural Science Foundation of China (32071149, 92157111, 82330028, 92357306, 92357307, 82170891, 32471175), the Strategic Priority Research Program of the Chinese Academy of Sciences (XDB39020800), Noncommunicable Chronic Diseases-National Science and Technology Major Project (2024ZD0530100), and Talent Plan of Shanghai Branch-Chinese Academy of Sciences (CASSHB-QNPD-2023-019).

Reference

1. Vandewalle J, Luypaert A, De Bosscher K, and Libert C. Therapeutic Mechanisms of Glucocorticoids. *Trends Endocrinol Metab.* 2018;29(1):42-54.
2. Smith TJ, and Hegedus L. Graves' Disease. *N Engl J Med.* 2016;375(16):1552-65.
3. Oray M, Abu Samra K, Ebrahimiadib N, Meese H, and Foster CS. Long-term side effects of glucocorticoids. *Expert Opin Drug Saf.* 2016;15(4):457-65.
4. Macfarlane DP, Forbes S, and Walker BR. Glucocorticoids and fatty acid metabolism in humans: fuelling fat redistribution in the metabolic syndrome. *J Endocrinol.* 2008;197(2):189-204.
5. Thuzar M, Law WP, Ratnasingam J, Jang C, Dimeski G, and Ho KKY. Glucocorticoids suppress brown adipose tissue function in humans: A double-blind placebo-controlled study. *Diabetes Obes Metab.* 2018;20(4):840-8.
6. Farmer SR. Transcriptional control of adipocyte formation. *Cell Metab.* 2006;4(4):263-73.
7. Steger DJ, Grant GR, Schupp M, Tomaru T, Lefterova MI, Schug J, et al. Propagation of adipogenic signals through an epigenomic transition state. *Gene Dev.* 2010;24(10):1035-44.
8. Park YK, and Ge K. Glucocorticoid Receptor Accelerates, but Is Dispensable for, Adipogenesis. *Mol Cell Biol.* 2017;37(2).
9. Bauerle KT, Hutson I, Scheller EL, and Harris CA. Glucocorticoid Receptor Signaling Is Not Required for In Vivo Adipogenesis. *Endocrinology.* 2018;159(5):2050-61.
10. Glantschnig C, Mattijssen F, Vogl ES, Khan AA, Garcia MR, Fischer K, et al. The

glucocorticoid receptor in brown adipocytes is dispensable for control of energy homeostasis. *Embo Rep.* 2019;20(11).

11. Ping YQ, Mao C, Xiao P, Zhao RJ, Jiang Y, Yang Z, et al. Structures of the glucocorticoid-bound adhesion receptor GPR97-G(o) complex. *Nature.* 2021;589(7843):620-6.
12. Siersbaek R, Nielsen R, John S, Sung MH, Baek S, Loft A, et al. Extensive chromatin remodelling and establishment of transcription factor 'hotspots' during early adipogenesis. *EMBO J.* 2011;30(8):1459-72.
13. Lee JE, Schmidt H, Lai B, and Ge K. Transcriptional and Epigenomic Regulation of Adipogenesis. *Mol Cell Biol.* 2019;39(11).
14. Mashtalir N, D'Avino AR, Michel BC, Luo J, Pan J, Otto JE, et al. Modular Organization and Assembly of SWI/SNF Family Chromatin Remodeling Complexes. *Cell.* 2018;175(5):1272-88 e20.
15. Pedersen TÅ, Kowenz-Leutz E, Leutz A, and Nerlov C. Cooperation between C/EBPα TBP/TFIIB and SWI/SNF recruiting domains is required for adipocyte differentiation. *Gene Dev.* 2001;15(23):3208-16.
16. Salma N, Xiao HG, Mueller E, and Imbalzano AN. Temporal recruitment of transcription factors and SWI/SNF chromatin-remodeling enzymes during adipogenic induction of the peroxisome proliferator-activated receptor γ nuclear hormone receptor. *Mol Cell Biol.* 2004;24(11):4651-63.
17. Wanior M, Preuss F, Ni XM, Krämer A, Mathea S, Göbel T, et al. Pan-SMARCA/PB1 Bromodomain Inhibitors and Their Role in Regulating Adipogenesis. *J Med Chem.* 2020;63(23):14680-99.
18. Park YK, Lee JE, Yan Z, McKernan K, O'Haren T, Wang W, et al. Interplay of BAF and MLL4 promotes cell type-specific enhancer activation. *Nat Commun.* 2021;12(1):1630.
19. Casamayor A, Torrance PD, Kobayashi T, Thorner J, and Alessi DR. Functional counterparts of mammalian protein kinases PDK1 and SGK in budding yeast. *Curr Biol.* 1999;9(4):186-97.
20. Park J, Leong ML, Buse P, Maiyar AC, Firestone GL, and Hemmings BA. Serum and glucocorticoid-inducible kinase (SGK) is a target of the PI 3-kinase-stimulated signaling pathway. *EMBO J.* 1999;18(11):3024-33.
21. Garcia-Martinez JM, and Alessi DR. mTOR complex 2 (mTORC2) controls hydrophobic motif phosphorylation and activation of serum- and glucocorticoid-induced protein kinase 1 (SGK1). *Biochem J.* 2008;416(3):375-85.
22. Malik N, Macartney T, Hornberger A, Anderson KE, Tovell H, Prescott AR, et al. Mechanism of activation of SGK3 by growth factors via the Class 1 and Class 3 PI3Ks. *Biochem J.* 2018;475(1):117-35.
23. Tessier M, and Woodgett JR. Role of the Phox homology domain and phosphorylation in activation of serum and glucocorticoid-regulated kinase-3. *J Biol Chem.* 2006;281(33):23978-89.
24. Malik N, Nirujogi RS, Peltier J, Macartney T, Wightman M, Prescott AR, et al. Phosphoproteomics reveals that the hVPS34 regulated SGK3 kinase specifically phosphorylates endosomal proteins including Syntaxin-7, Syntaxin-12, RFIP4 and WDR44. *Biochem J.* 2019;476(20):3081-107.

25. Gasser JA, Inuzuka H, Lau AW, Wei W, Beroukhim R, and Toker A. SGK3 mediates INPP4B-dependent PI3K signaling in breast cancer. *Mol Cell.* 2014;56(4):595-607.
26. Bago R, Sommer E, Castel P, Crafter C, Bailey FP, Shpiro N, et al. The hVps34-SGK3 pathway alleviates sustained PI3K/Akt inhibition by stimulating mTORC1 and tumour growth. *EMBO J.* 2016;35(17):1902-22.
27. He P, Lee SJ, Lin S, Seidler U, Lang F, Fejes-Toth G, et al. Serum- and glucocorticoid-induced kinase 3 in recycling endosomes mediates acute activation of Na+/H+ exchanger NHE3 by glucocorticoids. *Mol Biol Cell.* 2011;22(20):3812-25.
28. McCormick JA, Feng Y, Dawson K, Behne MJ, Yu B, Wang J, et al. Targeted disruption of the protein kinase SGK3/CISK impairs postnatal hair follicle development. *Mol Biol Cell.* 2004;15(9):4278-88.
29. Tsai SF, Hung HC, Shih MM, Chang FC, Chung BC, Wang CY, et al. High-fat diet-induced increases in glucocorticoids contribute to the development of non-alcoholic fatty liver disease in mice. *FASEB J.* 2022;36(1):e22130.
30. Jeffery E, Church CD, Holtrup B, Colman L, and Rodeheffer MS. Rapid depot-specific activation of adipocyte precursor cells at the onset of obesity. *Nat Cell Biol.* 2015;17(4):376-85.
31. Vasudevan KM, Barbie DA, Davies MA, Rabinovsky R, McNear CJ, Kim JJ, et al. AKT-independent signaling downstream of oncogenic PIK3CA mutations in human cancer. *Cancer Cell.* 2009;16(1):21-32.
32. He B, Bie Q, Zhao R, Yan Y, Dong G, Zhang B, et al. Arachidonic acid released by PIK3CA mutant tumor cells triggers malignant transformation of colonic epithelium by inducing chromatin remodeling. *Cell Rep Med.* 2024;5(5):101510.
33. Wang M, Liu J, Liao X, Yi Y, Xue Y, Yang L, et al. The SGK3-Catalase antioxidant signaling axis drives cervical cancer growth and therapy resistance. *Redox Biol.* 2023;67:102931.
34. Pokorny D, Truebestein L, Fleming KD, Burke JE, and Leonard TA. In vitro reconstitution of Sgk3 activation by phosphatidylinositol 3-phosphate. *J Biol Chem.* 2021;297(2):100919.
35. Timmermans S, Souffriau J, and Libert C. A General Introduction to Glucocorticoid Biology. *Front Immunol.* 2019;10:1545.
36. Liu D, Yang XH, and Zhou SY. Identification of CISK, a new member of the SGK kinase family that promotes IL-3-dependent survival. *Current Biology.* 2000;10(19):1233-6.
37. Wang QA, Tao C, Gupta RK, and Scherer PE. Tracking adipogenesis during white adipose tissue development, expansion and regeneration. *Nat Med.* 2013;19(10):1338-44.
38. Zannas AS, and Chrousos GP. Glucocorticoid signaling drives epigenetic and transcription factors to induce key regulators of human parturition. *Sci Signal.* 2015;8(400):fs19.
39. Vockley CM, D'Ippolito AM, McDowell IC, Majoros WH, Safi A, Song L, et al. Direct GR Binding Sites Potentiate Clusters of TF Binding across the Human Genome. *Cell.* 2016;166(5):1269-81 e19.
40. Tomiyama K, Nakata H, Sasa H, Arimura S, Nishio E, and Watanabe Y. Wortmannin, a specific phosphatidylinositol 3-kinase inhibitor, inhibits adipocytic differentiation of 3T3-

L1 cells. *Biochem Biophys Res Commun.* 1995;212(1):263-9.

41. Song W, Postoak JL, Yang G, Guo X, Pua HH, Bader J, et al. Lipid kinase PIK3C3 maintains healthy brown and white adipose tissues to prevent metabolic diseases. *Proc Natl Acad Sci U S A.* 2023;120(1):e2214874120.
42. Cai K, El-Merahbi R, Loeffler M, Mayer AE, and Sumara G. Ndrg1 promotes adipocyte differentiation and sustains their function. *Sci Rep.* 2017;7(1):7191.
43. Yao LJ, McCormick JA, Wang J, Yang KY, Kidwai A, Colussi GL, et al. Novel role for SGK3 in glucose homeostasis revealed in SGK3/Akt2 double-null mice. *Mol Endocrinol.* 2011;25(12):2106-18.
44. Sandu C, Rexhepaj R, Grahammer F, McCormick JA, Henke G, Palmada M, et al. Decreased intestinal glucose transport in the sgk3-knockout mouse. *Pflugers Arch.* 2005;451(3):437-44.
45. Bohmer C, Palmada M, Kenngott C, Lindner R, Klaus F, Laufer J, et al. Regulation of the epithelial calcium channel TRPV6 by the serum and glucocorticoid-inducible kinase isoforms SGK1 and SGK3. *FEBS Lett.* 2007;581(29):5586-90.
46. Embark HM, Setiawan I, Poppendieck S, van de Graaf SF, Boehmer C, Palmada M, et al. Regulation of the epithelial Ca2+ channel TRPV5 by the NHE regulating factor NHERF2 and the serum and glucocorticoid inducible kinase isoforms SGK1 and SGK3 expressed in Xenopus oocytes. *Cell Physiol Biochem.* 2004;14(4-6):203-12.
47. Chang CA, Jen J, Jiang S, Sayad A, Mer AS, Brown KR, et al. Ontogeny and Vulnerabilities of Drug-Tolerant Persisters in HER2+ Breast Cancer. *Cancer Discov.* 2022;12(4):1022-45.
48. Zhou B, Kreuzer J, Kumsta C, Wu L, Kamer KJ, Cedillo L, et al. Mitochondrial Permeability Uncouples Elevated Autophagy and Lifespan Extension. *Cell.* 2019;177(2):299-314 e16.
49. Cheng L, Hu J, Zhang L, Shen N, Chen H, and Zhang F. Repurposing Lenvatinib as A Potential Therapeutic Agent against Thyroid Eye Disease by Suppressing Adipogenesis in Orbital Adipose Tissues. *Pharmaceuticals (Basel).* 2022;15(11).

Figures

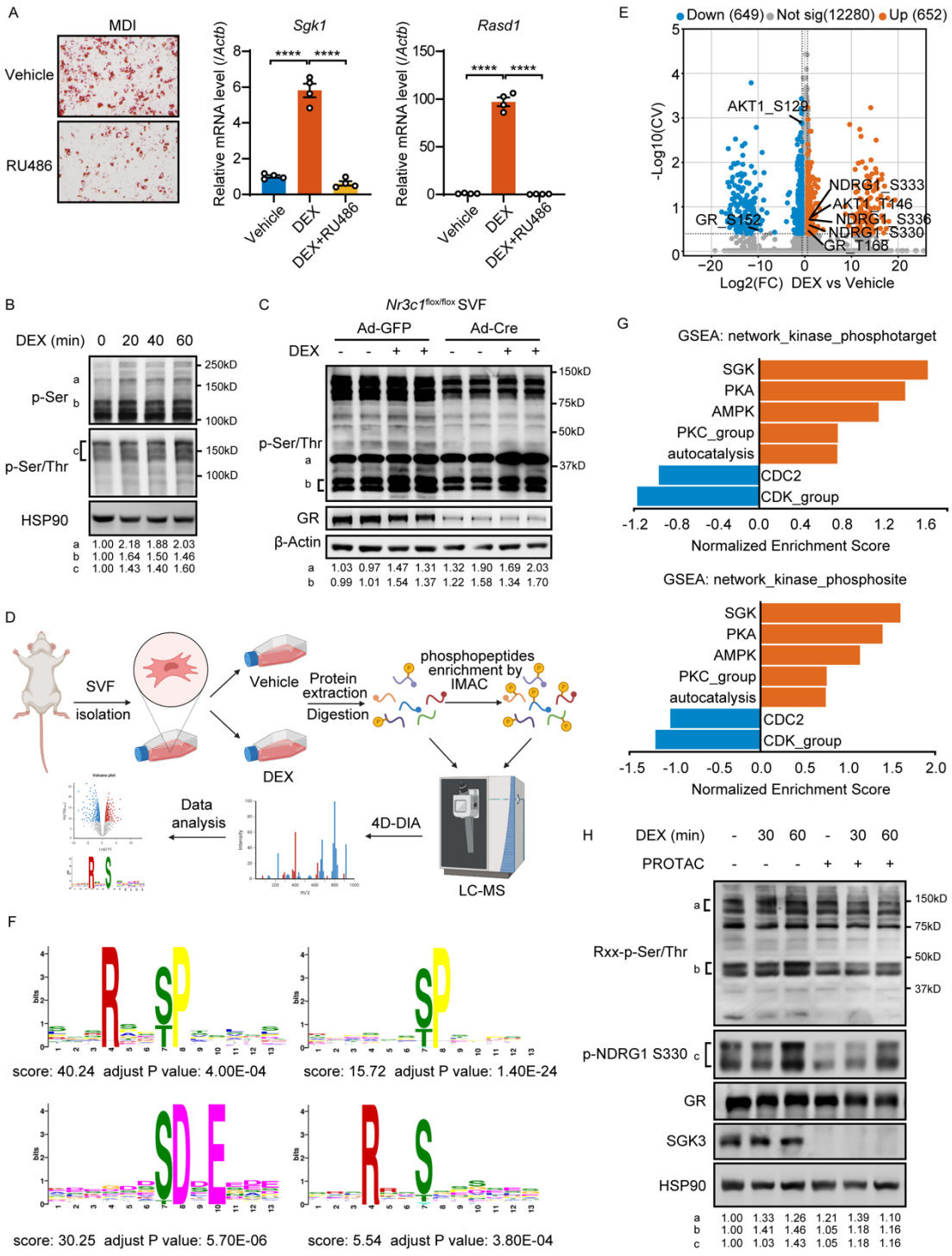

Figure 1. SGK3 is essential for protein phosphorylation in response to glucocorticoid stimulation.

(**A**) Representative images of Oil Red O staining of differentiated preadipocytes

treated with vehicle or RU486 (left), Scale bar: 200 μm. mRNA level of GR targets, *Sgk1* (middle) and *Rasd1* (right), in preadipocytes treated with DEX or DEX and RU486 for 24h. *n* = 4 from different culture wells. (**B**) Protein phosphorylation in preadipocytes induced by DEX treatment at various time points. Relative band intensities were quantified (normalized to HSP90) and are shown below the figure. (**C**) Protein phosphorylation in GFP- or Cre-expressed *Nr3c1*$^{flox/flox}$ primary SVF cells induced by DEX treatment. Relative band intensities were quantified (normalized to β-Actin) and are shown below the figure. (**D**) Experimental workflow to identify glucocorticoid induced protein phosphorylation. (**E**) Volcano plot illustrating DEX-induced phosphorylation alterations. (**F**) Motif analysis of DEX induced phosphorylation sites. (**G**) GSEA analysis of DEX induce phosphorylation sites with datasets of network_kinase_phosphotarget and network_kinase_phosphosite. (**H**) SGK3 deficiency attenuates DEX-induced phosphorylation of RxxS/T peptides and phosphorylation of NDRG1 at serine 330. Relative band intensities were quantified (normalized to HSP90) and are shown below the figure. Identical sample aliquots were loaded on separate gels for immunoblotting analysis in Figures B, C and H. Data in (**A**) were represented as mean ± SEM, and One-way ANOVA was used for statistical analysis. ****$P < 0.0001$.

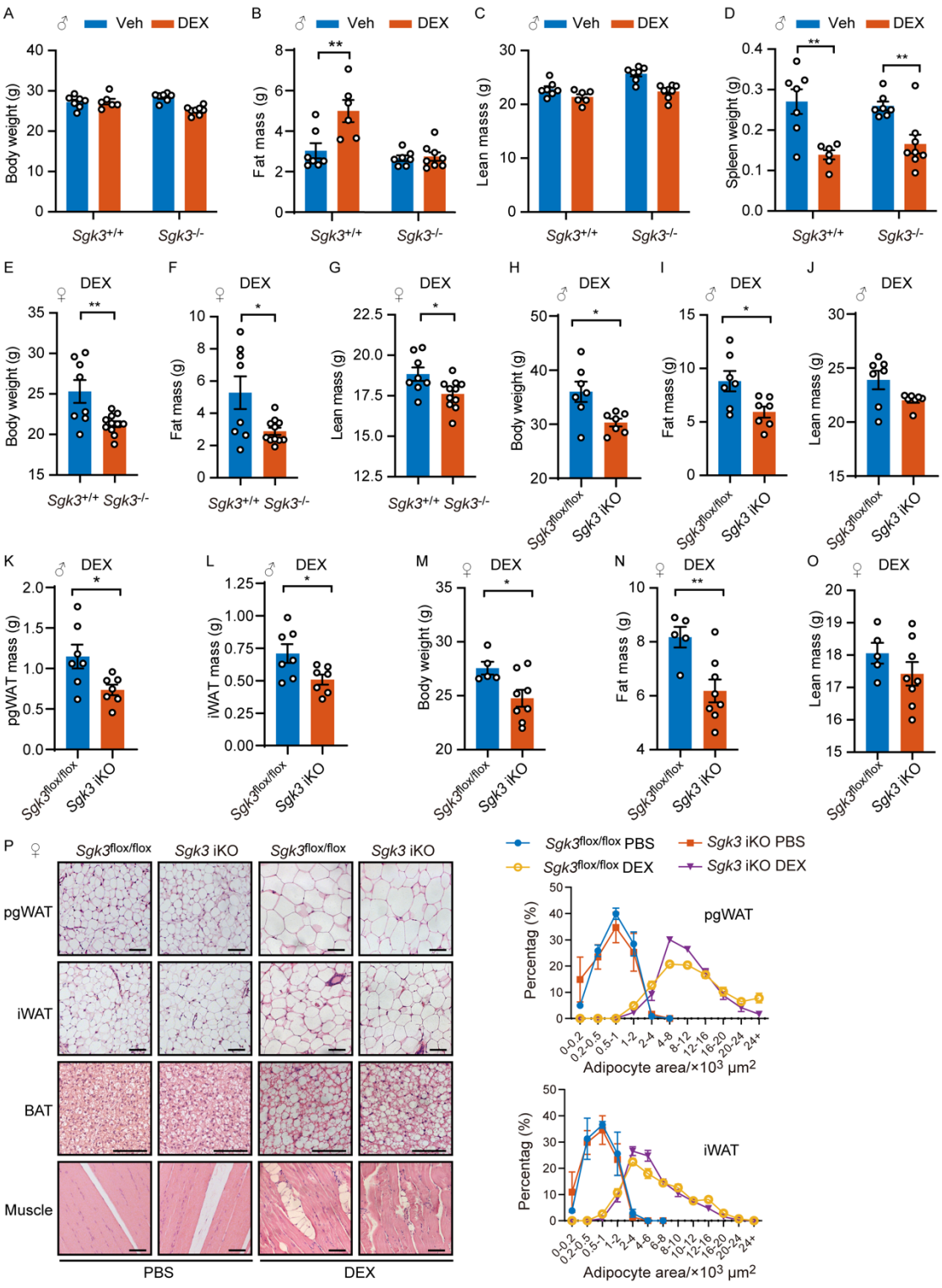

Figure 2. *Sgk3*-deficient mice are protected from glucocorticoid-induced obesity.

(**A-D**) Body weight (**A**), fat mass (**B**), lean mass (**C**), and spleen weight (**D**) of

vehicle or DEX-treated *Sgk3*$^{+/+}$ and *Sgk3*$^{-/-}$ male mice over 28 days. *n* = 7 for *Sgk3*$^{+/+}$ (Veh), *n* = 6 for *Sgk3*$^{+/+}$ (DEX), *n* = 7 for *Sgk3*$^{-/-}$ (Veh), *n* = 8 for *Sgk3*$^{-/-}$ (DEX). (**E-G**) Body weight (**E**), fat mass (**F**), and lean mass (**G**) of DEX-treated *Sgk3*$^{+/+}$ and *Sgk3*$^{-/-}$ female mice over 28 days. *n* = 8 for *Sgk3*$^{+/+}$, *n* = 11 for *Sgk3*$^{-/-}$. (**H-L**) Body weight (**H**), Fat mass (**I**), Lean mass (**J**), pgWAT weight (**K**) and iWAT weight (**L**) of DEX-treated *Sgk3*$^{flox/flox}$ and *Sgk3* iKO (inducible knock out by tamoxifen) male mice over 32 days. *n* = 7 for each group. (**M-O**) Body weight (**M**), Fat mass (**N**) and Lean mass (**O**) of DEX-treated *Sgk3*$^{flox/flox}$ and *Sgk3* iKO female mice over 28 days. *n* = 5 for *Sgk3*$^{flox/flox}$ mice, *n* = 8 for *Sgk3* iKO mice. (**P**) Representative images of H&E staining of pgWAT, iWAT, BAT and muscle of PBS or DEX-treated *Sgk3*$^{flox/flox}$ and *Sgk3* iKO female mice over 28 days. Scale bar: 100 μm. Related quantifications of adipocyte area of pgWAT and iWAT. *n* = 5 mice per group (>200 adipocytes are quantified for each mouse). Data in **A**-**D** were represented as mean ± SEM, and Two-way ANOVA was used for statistical analysis. Data in **E**-**O** were represented as mean ± SEM, and unpaired two-tailed T-test was used for statistical analysis. Data in **P** were represented as mean ± SEM. **P* < 0.05, ***P* < 0. 01.

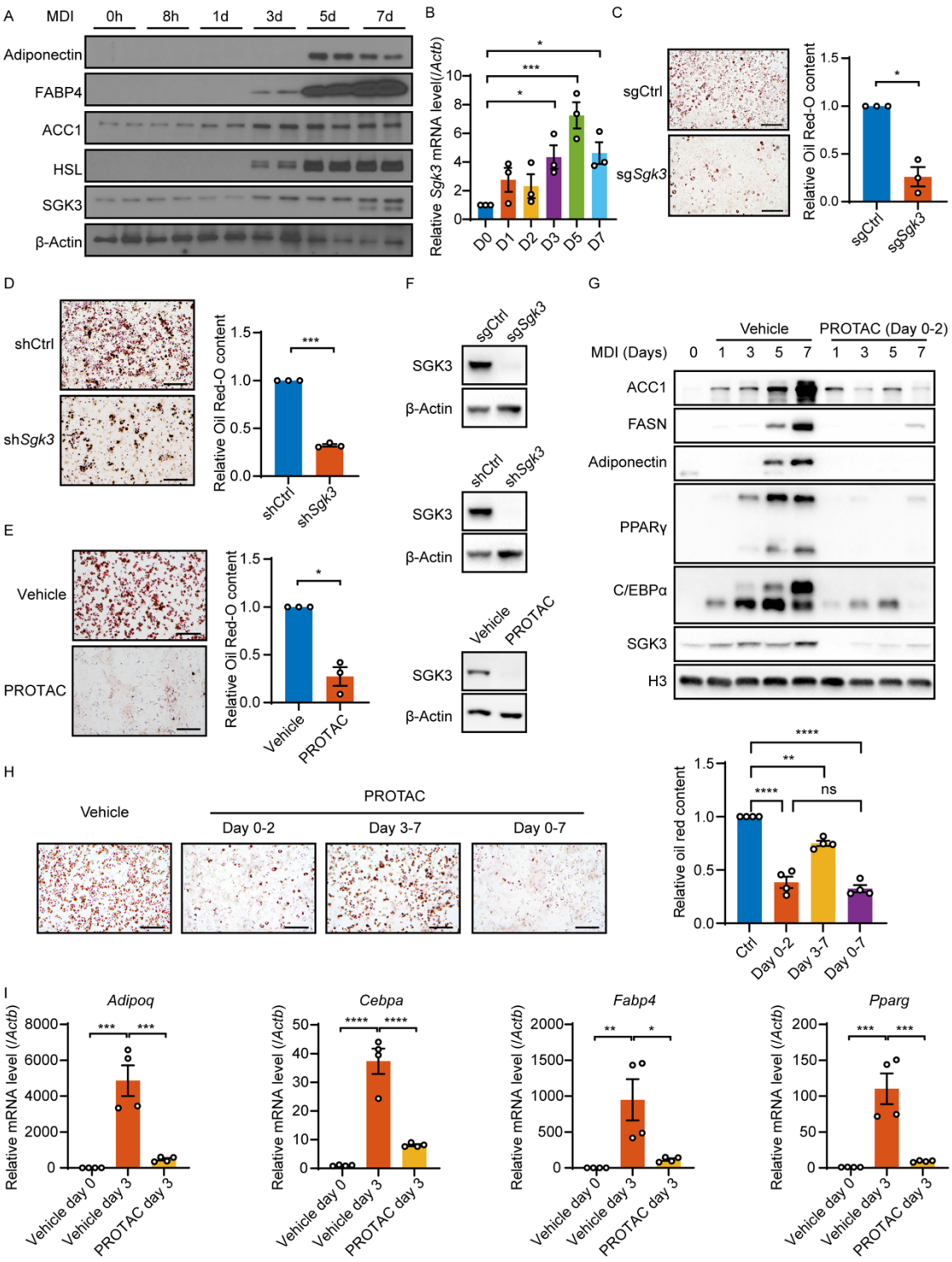

Figure 3. SGK3 regulates adipogenesis.

(**A**) Protein level of SGK3, Adiponectin, FABP4, ACC1 and HSL in 3T3-L1 preadipocytes during adipogenic differentiation. (**B**) mRNA level of *Sgk3* in 3T3-L1 preadipocytes during adipogenic differentiation. *n* = 3 independent assays.

(**C**-**E**) Representative images of Oil Red O staining and related quantifications of differentiated *Sgk3* knock out (**C**), *Sgk3* knock down (**D**), and vehicle or SGK3 PROTAC treated (**E**) preadipocytes on day 7. Scale bar: 200 μm. *n* = 3 independent assays. (**F**) Protein level of SGK3 in *Sgk3* knock out, knock down and SGK3 PROTAC-treated preadipocytes. (**G**) Protein level of ACC1, FASN, Adiponectin, PPARγ, C/EBPα and SGK3 during preadipocyte differentiation with or without SGK3 PROTAC treatment during first 2 days. (**H**) Representative images of Oil Red O staining (left) and related quantifications (right) of differentiated preadipocytes with or without SGK3 PROTAC treatment during indicated times on day 7. Scale bar: 200 μm. *n* = 4 independent assays. (**I**) mRNA level of *Adipoq*, *Cebpa*, *Fabp4* and *Pparg* during preadipocyte differentiation with or without SGK3 PROTAC treatment during the first 2 days. *n* = 4 samples from different culture wells. Data in **B, H**-**I** were represented as mean ± SEM, and One-way ANOVA was used for statistical analysis. Data in **C**-**E** were represented as mean ± SEM, and paired two-tailed T-test was used for statistical analysis. "ns" indicates no significance, **P* < 0.05, ***P* < 0.01, ****P* < 0.001, *****P* < 0.0001.

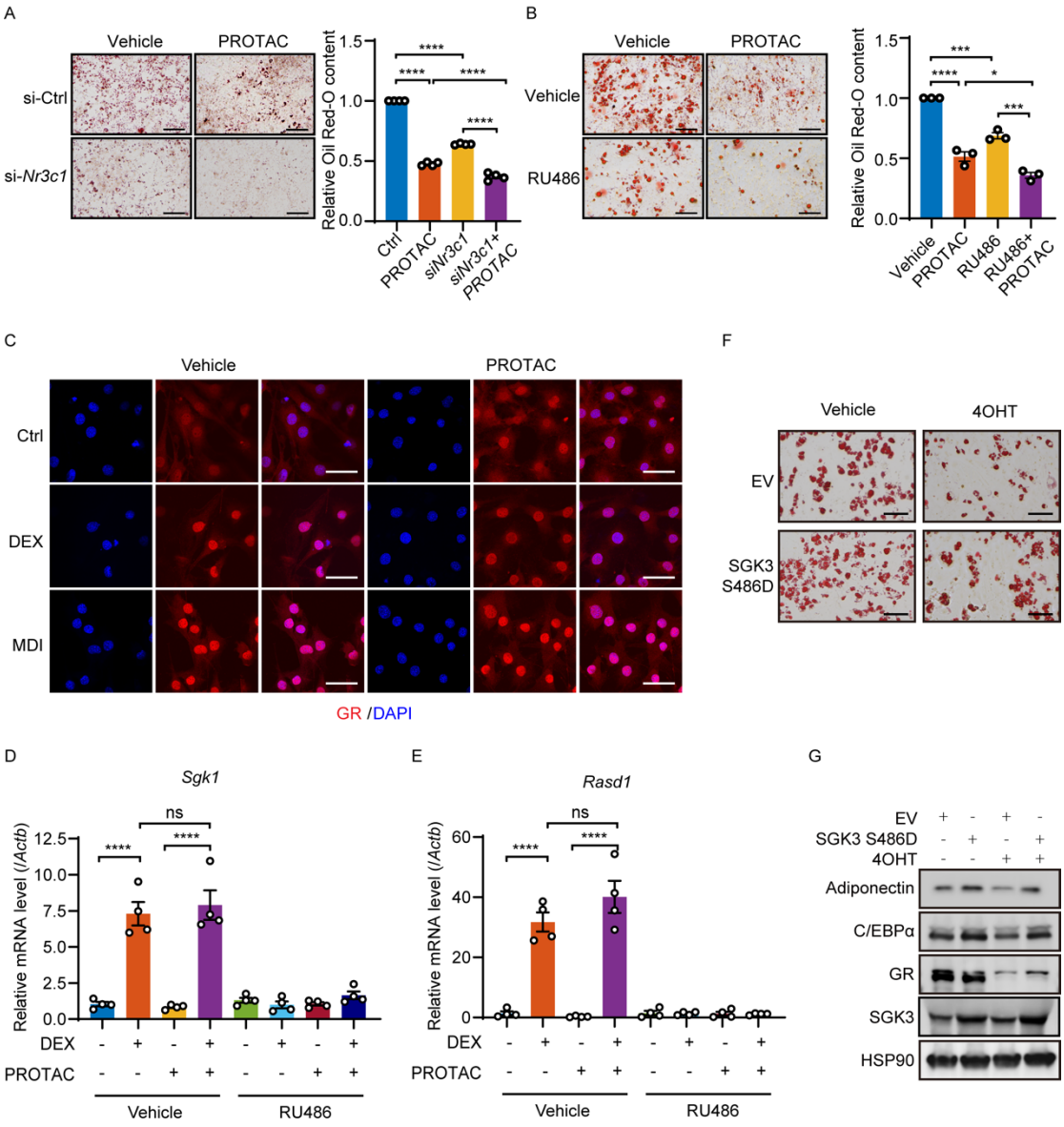

Figure 4. SGK3 regulates adipogenesis independently of GR signaling.

(**A**) Representative images of Oil Red O staining and related quantifications of differentiated preadipocytes transfected Ctrl or *Nr3c1* siRNA and/or treated with SGK3 PROTAC on day 7. Scale bar: 200 μm. *n* = 4 independent assays. (**B**) Representative images of Oil Red O staining and related quantifications of differentiated preadipocytes treated with RU486 and/or SGK3 PROTAC on day 21. Scale bar: 200 μm. *n* = 3 independent assays. (**C**) Representative

immunofluorescence images of GR in SVF cells treated as indicated. Scale bar: 50 μm. (**D** and **E**) mRNA level of *Sgk1* (**D**) and *Rasd1* (**E**) in preadipocytes treated with DEX, SGK3 PROTAC and RU486 as indicated. *n* = 4 samples from different culture wells. **(F)** Representative images of Oil Red O staining of differentiated preadipocytes with or without SGK3 S486D overexpression in control and GR deficient cells on day 7. Scale bar: 200 μm. **(G)** SGK3 S486D overexpression effects on protein levels of Adiponectin and C/EBPα on day 3 of differentiation in control and GR-deficient cells. Identical sample aliquots were loaded on separate gels for immunoblotting analysis in Figure G. Data in **A**-**B**, **D**-**E** were represented as mean ± SEM, and One-way ANOVA was used for statistical analysis. "ns" indicates no significance, **P* < 0.05, ****P* < 0.001, *****P* < 0.0001.

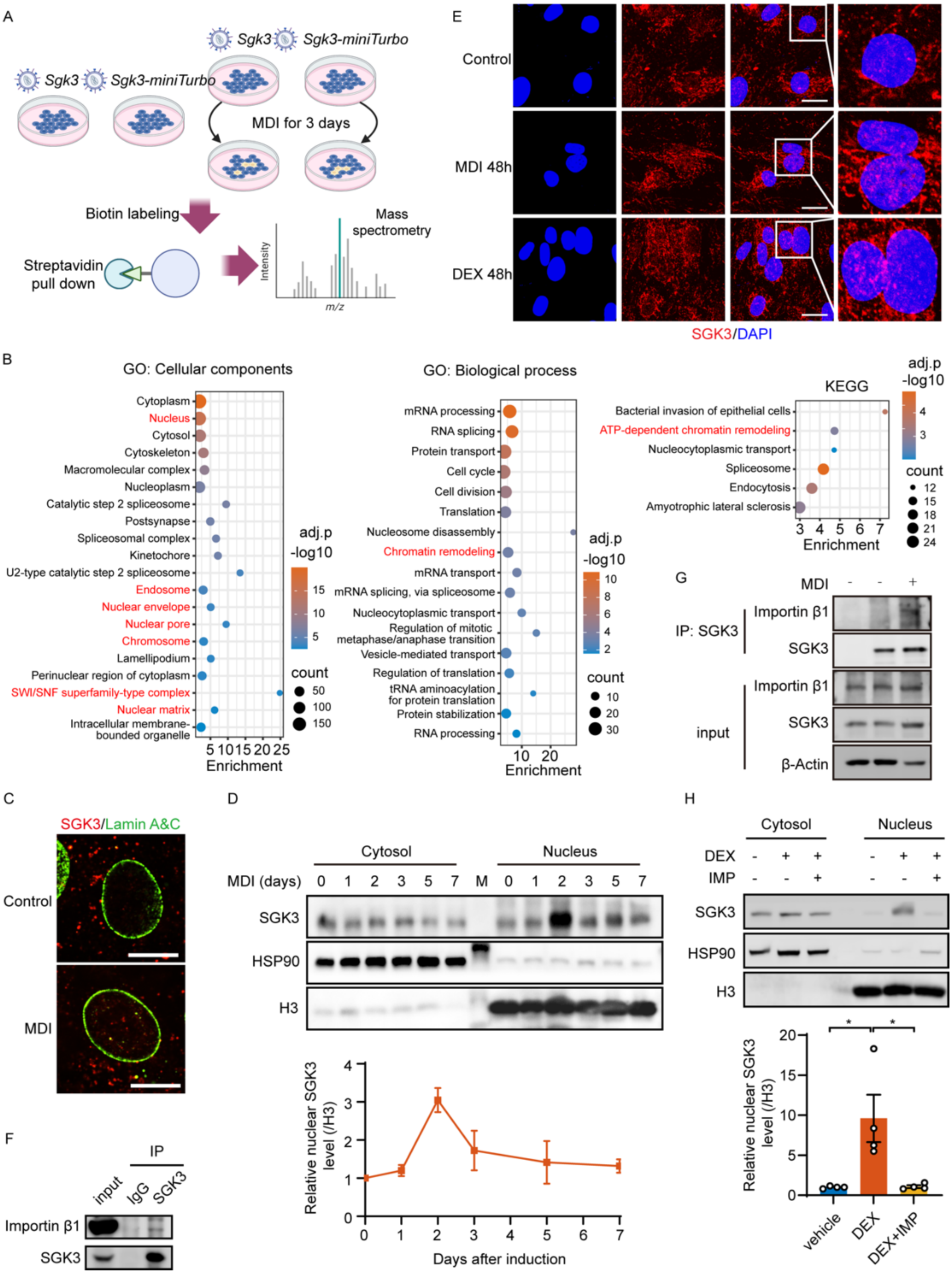

Figure 5. Glucocorticoid-induced nuclear SGK3 translocation during early stage of preadipocyte differentiation.

(**A**) Strategy for identifying SGK3-interacting proteins. (**B**) GO enrichment analysis of SGK3-interacting proteins. (**C**) Representative immunofluorescence

images of SGK3 and Lamin A&C in differentiating primary SVF cells on day 2. Scale bar: 20 μm. (**D**) Localization of SGK3 in the cytosol fraction and nucleus at indicated time points during preadipocyte differentiation and related quantifications (normalized to H3). *n* = 3 independent assays. (**E**) Representative immunofluorescence images of SGK3 in preadipocytes treated with MDI or DEX for 2 days. Scale bar: 20 μm. (**F**) Co-IP shows SGK3 and Importin β1 interaction in cells treated with MDI for 3 days. (**G**) Co-IP shows SGK3 and Importin β1 interaction in cells treated with or without MDI for 2 days. (**H**) DEX-induced nuclear translocation of SGK3 with or without IMP treatment and related quantifications (normalized to H3) over 2 days. *n* = 4 samples from different culture wells. Data in **D** were represented as mean ± SEM. Identical sample aliquots were loaded on separate gels for immunoblotting analysis in Figure D. Data in **H** were represented as mean ± SEM, and One-way ANOVA was used for statistical analysis. *$P < 0.05$.

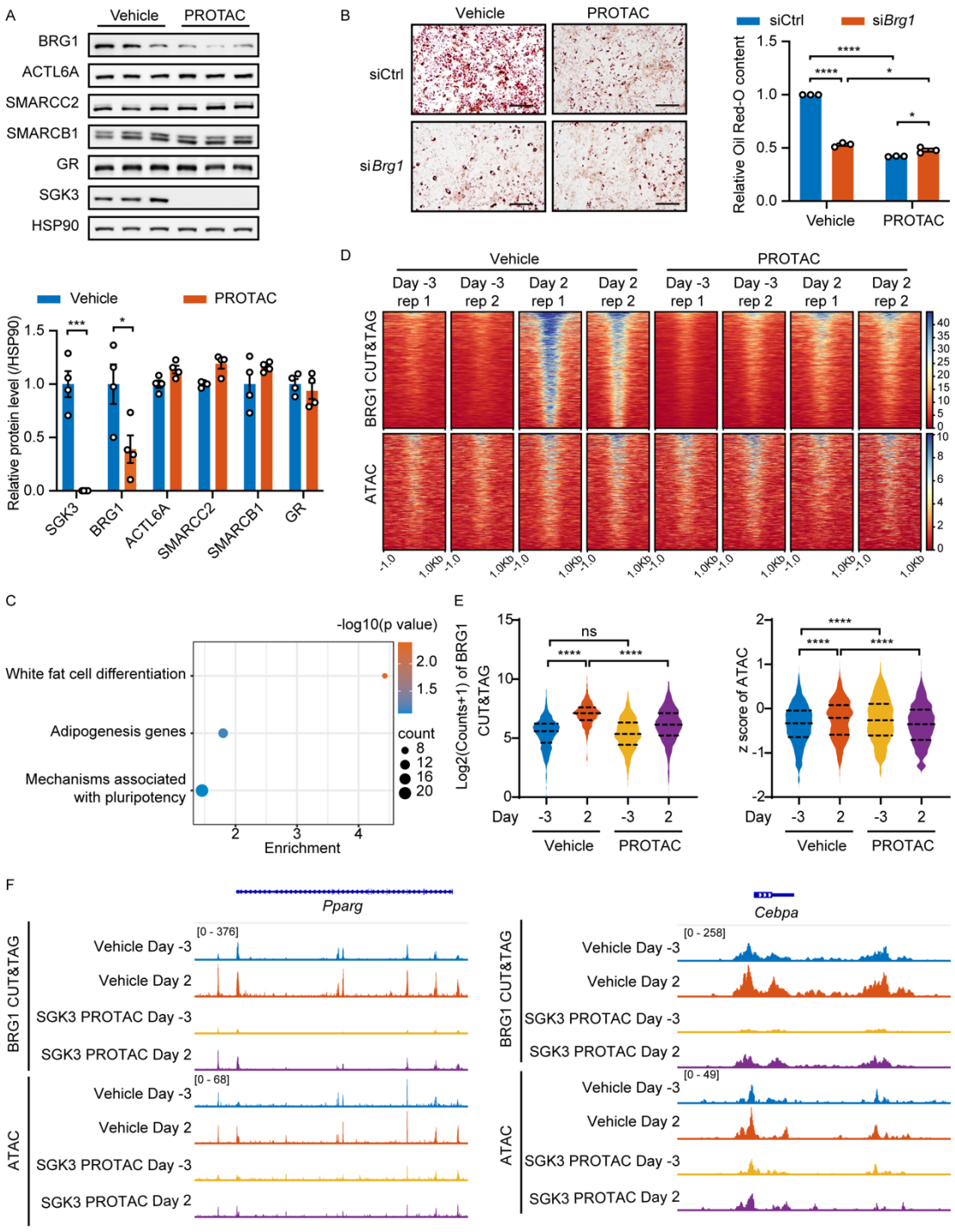

Figure 6. Deficiency of SGK3 impairs chromatin remodeling during preadipocyte differentiation.

(**A**) Representative western blot (upper) and related quantifications (lower) of BRG1, ACTL6A, SMARCC2, SMARCB1, GR and SGK3 in SGK3 PROTAC

treated preadipocytes. *n* = 4 samples from different culture wells. (**B**) Representative images of Oil Red O staining (left) and related quantifications (right) of differentiated preadipocytes transfected with Ctrl or *Brg1* siRNA and/or treated with SGK3 PROTAC on day 7. Scale bar: 200 μm. *n* =3 independent assays. (**C**) Enrichment analysis of genes nearby the regions of induced BRG1 occupation during preadipocyte differentiation. (**D**) Heatmap of BRG1 CUT&TAG (upper) and ATAC-seq (lower) signals with or without SGK3 PROTAC treatment during preadipocyte differentiation. (**E**) Quantification of BRG1 CUT&TAG signals and ATAC-seq signals in regions of induced BRG1 occupation during preadipocyte differentiation. *n* =1158 regions. (**F**) BRG1 CUT&TAG and ATAC-seq signals in the *Pparg* and *Cebpa* gene locus. Data in **A** are represented as mean ± SEM, and unpaired two tailed T-test was used for statistical analysis. Data in **B** were represented as mean ± SEM, and Two -way ANOVA was used for statistical analysis. Identical sample aliquots were loaded on separate gels for immunoblotting analysis in Figure A. Data in **E** were represented as mean and 25th to 75th percentile, and One-way ANOVA was used for statistical analysis. "ns" indicates no significance, **P* < 0.05, ****P* < 0.001, *****P* < 0.0001.

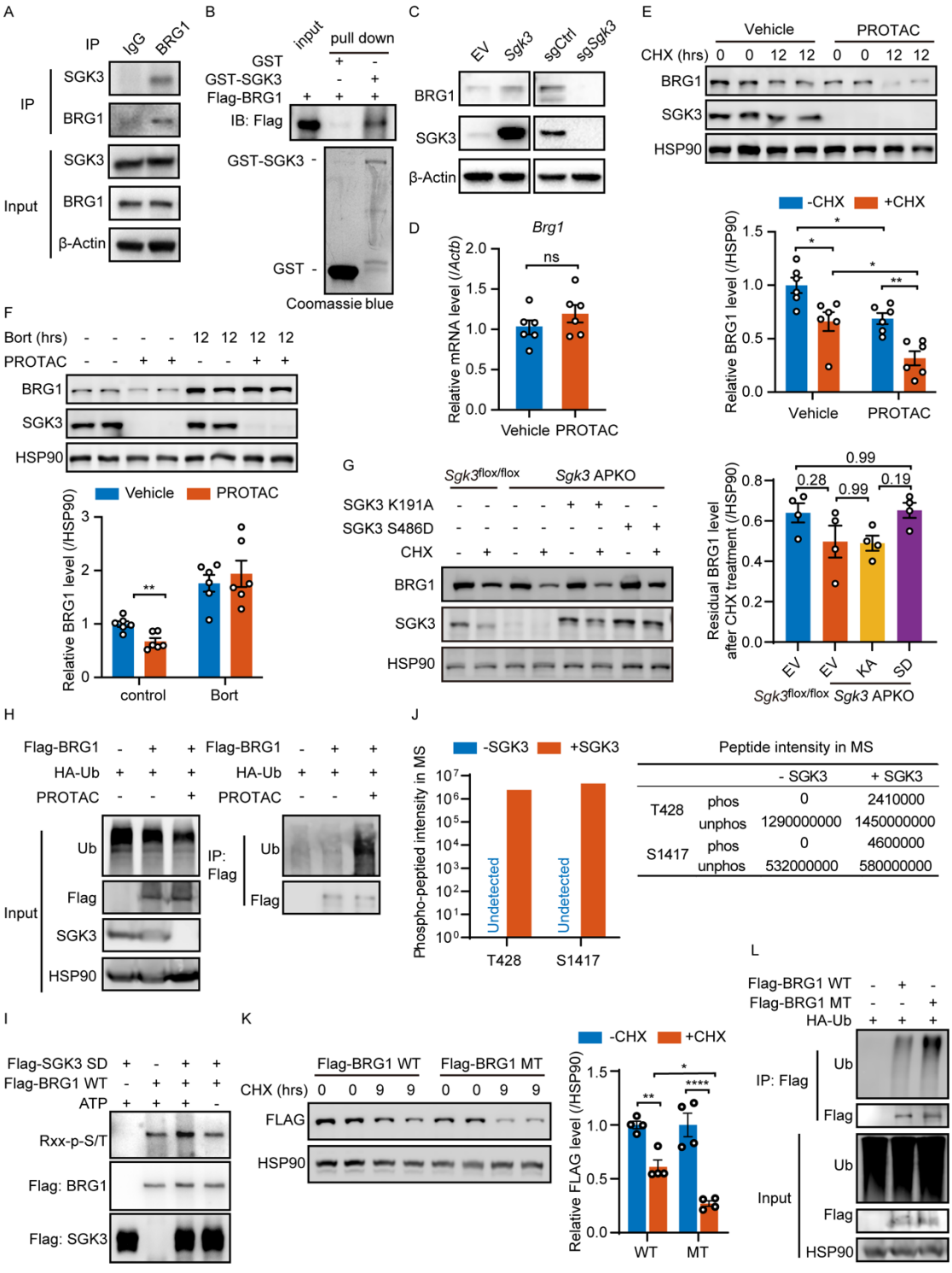

Figure 7. SGK3 regulates differentiation associated chromatin remodeling via BRG1.

(**A**) Co-IP assay indicates BRG1 interact with SGK3. (**B**) The direct interaction between SGK3 and BRG1 is detected by GST-Pull Down Assay. (**C**) Protein

level of BRG1 in *Sgk3* overexpression (left) or knock out (right) cells. (**D**) mRNA level of *Brg1* in SGK3 PROTAC treated cells. *n* = 6 samples from different culture wells. (**E** and **F**) Representative western blot of BRG1 protein levels (upper) and related quantifications (lower) in vehicle or SGK3 PROTAC treated preadipocytes are measured under cycloheximide (CHX) treatment (**E**) or bortezomib treatment (**F**), *n* = 6 samples from different culture wells. (**G**) Representative western blot of BRG1 protein levels (left) and related quantifications (right) in *Sgk3*$^{flox/flox}$ and *Sgk3* APKO SVF cells expressing either kinase-dead (K191A) or constitutively active (S486D) SGK3 mutants treated with CHX for 8h. *n* = 4 samples from different culture wells. (**H**) Ubiquitination level of Flag-BRG1 protein in HEK-293T cell with or without SGK3 PROTAC treatment. (**I**) *In vitro* kinase assay shows SGK3 directly phosphorylates the BRG1. (**J**) Intensity of 428-threonine and 1417-serine phosphorylated peptides of human BRG1 protein quantified by MS. (**K**) Representative western blot of Wild-type (WT) and T428A/S1417A mutant human BRG1 protein levels (left) and related quantifications (right) are measured under CHX treatment in HEK293T cells. *n* = 4 samples from different culture wells. (**L**) Ubiquitination level of Wild-type (WT) and T428A/S1417A mutant human BRG1 proteins in HEK293T cells treated with or without SGK3 PROTAC. Data in **D** were represented as mean ± SEM, and unpaired two-tailed T-test was used for statistical analysis. Data in **E** and **K** were represented as mean ± SEM, and Two-way ANOVA was used for statistical analysis. Data in **F** were represented

as mean ± SEM, and multiple T-tests were used for statistical analysis. Data in **G** were represented as mean ± SEM, and One-way ANOVA was used for statistical analysis. Identical sample aliquots were loaded on separate gels for immunoblotting analysis in Figures H and L. Data in **J** were represented as value. "ns" indicates no significance, **P* < 0.05, ***P* < 0.01, ****P* < 0.001, *****P* < 0.0001.

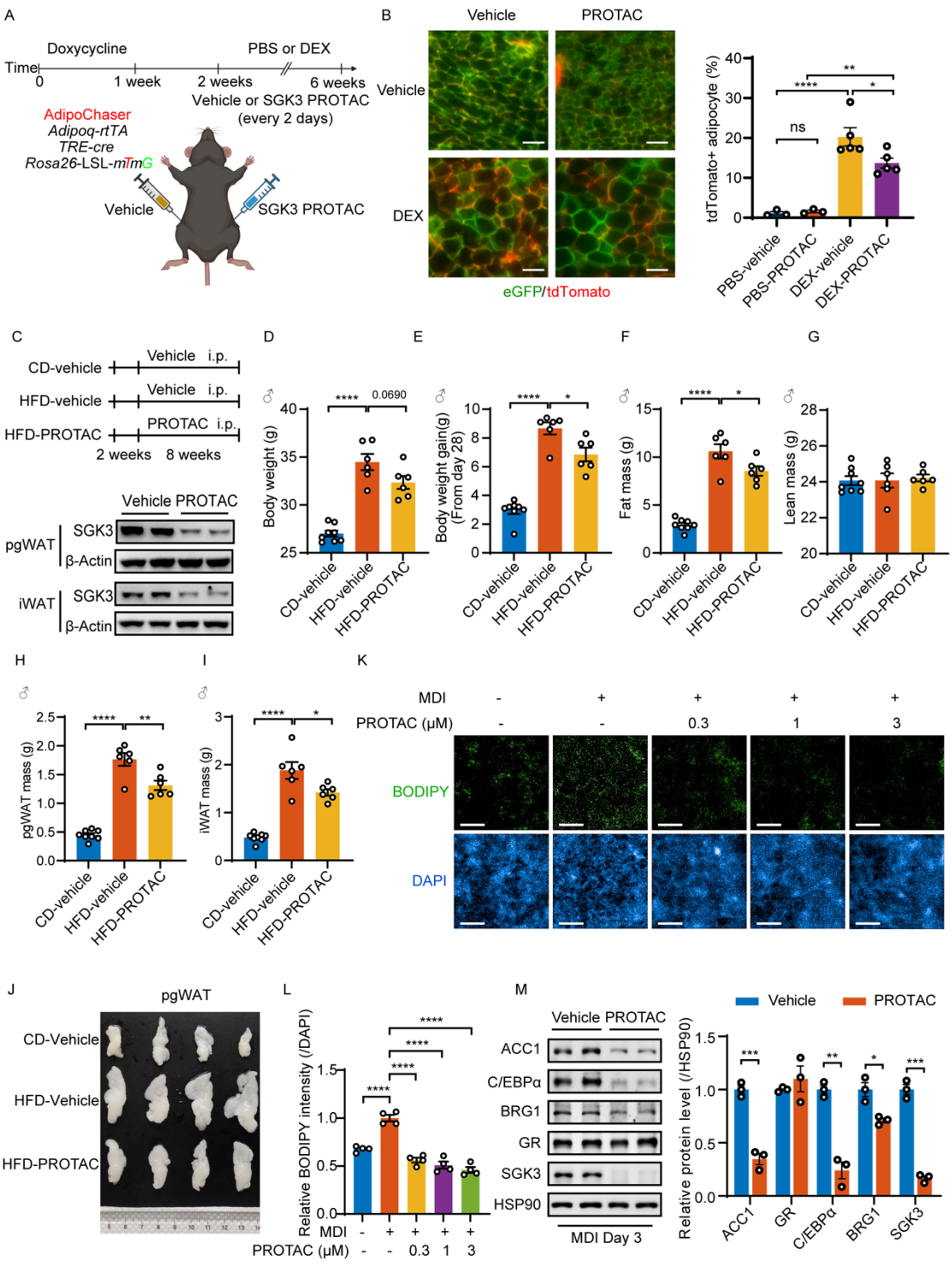

Figure 8. Pharmaceutical targeting of SGK3 attenuates HFD-induced obesity in mice, adipogenesis *in vivo* and in human cells.

(**A**) Experimental workflow to examine the function of SGK3 in adipogenesis *in vivo* using AdipoChaser-*mT/mG* mice. (**B**) Effects of SGK3 PROTAC on

adipogenesis in iWAT with or without DEX treatment. (Left) Representative images of iWAT sections showing pre-existing (green) and newborn (red) adipocytes. (Right) Quantification of newborn adipocytes per field. Scale bar: 100 μm. *n* = 3 for PBS-vehicle and PBS-PROTAC groups, *n* = 5 for DEX-vehicle and DEX-PROTAC groups. (**C**) Experimental workflow (upper) to examine the function of SGK3 PROTAC in the treatment of HFD induced obesity. Western blot (lower) was used for detecting SGK3 in pgWAT and iWAT of control and SGK3 PROTAC-treated mice. (**D**-**I**) Body weight (**D**), Body weight change (**E**), Fat mass (**F**), Lean mass (**G**), pgWAT weight (**H**) and iWAT weight (**I**) of mice fed with chow diet and HFD fed with or without SGK3 PROTAC treatment. *n* = 8 for CD-vehicle, *n* = 6 for HFD-vehicle and HFD-PROTAC. (**J**) Representative images of pgWAT of mice fed with chow diet and HFD fed with or without SGK3 PROTAC treatment. (**K** and **L**) Representative images of BODIPY staining (**K**) and related quantifications (**L**) of differentiated human preadipocytes treated with SGK3 PROTAC at indicated concentrations. Scale bar: 500 μm. *n* = 4 samples from different culture wells. (**M**) Representative western blot and related quantifications of ACC1, C/EBPα, BRG1, GR, SGK3 in differentiating human preadipocytes with or without SGK3 PROTAC treatment on day 3. *n* = 3 samples from different culture wells. Identical sample aliquots were loaded on separate gels for Western blotting analysis in Figure M. Data in **B**, **D**-**I**, **L** and **M** were represented as mean ± SEM, and One-way ANOVA was used for statistical analysis. **P* < 0.05, ***P* < 0. 01, ****P* < 0. 001, *****P* < 0. 0001.